Role of relapse and multiple time delays in shaping Nipah virus epidemic dynamics: a mathematical modeling study

Sarita Bugalia[a,*], Hao Wang[b], Liliana C.M. Salvador[a]
[a] School of Animal & Comparative Biomedical Sciences,
College of Agriculture, Life and Environmental Sciences,
The University of Arizona, Tucson, Arizona, 85721, USA
[b] Interdisciplinary Lab for Mathematical Ecology & Epidemiology,
Department of Mathematical and Statistical Sciences,
University of Alberta, Edmonton, T6G 2G1, Canada
[*] Corresponding Author: bugalias@arizona.edu

Abstract

Nipah virus (NiV) is a sporadic yet extremely deadly zoonotic pathogen, with reported case fatality rates of 40%-75% in impacted areas. Prolonged incubation, documented relapse, and delayed-onset encephalitis following apparent recovery indicate that NiV dynamics are influenced by intricate temporal processes. However, mechanistic contributions of these processes to epidemic persistence remain poorly understood. In this study, we develop and analyze a delay differential equation model for NiV transmission that explicitly incorporates incubation delay, relapse, and post-recovery delay effects. We compute a primary-transmission reproduction threshold (R_0), characterize the disease-free and endemic equilibria, and analyze their stability, including delay-induced Hopf bifurcations. We show that relapse modifies the endemic-equilibrium existence condition, so an endemic equilibrium is not determined solely by the classical threshold criterion $R_0 = 1$. We calibrate the model to NiV incidence data from Bangladesh (2001-2024) and perform simulations and sensitivity analyses to evaluate the effects of relapse and delays across epidemiological scenarios. Results indicate that sustained oscillations occur only under hypothetical parameter regimes, suggesting that delay-induced periodic outbreaks are unlikely under empirically informed conditions. Scenario analyses demonstrate that relapse and encephalitis-related delays predominantly influence post-peak dynamics, while incubation delay alters the time and intensity of the epidemic peak. We also introduce a relapse-driven replenishment fraction to quantify contribution of relapse to continued transmission, demonstrating its growing significance following the first outbreak peak. Overall, our results identify relapse as a key mechanism for epidemic persistence and underscore the importance of incorporating relapse and biological time delays into epidemiological modeling and public health strategies.

Keywords: Nipah virus, Mathematical modeling, Time delays, Relapse rate, Hopf bifurcation, Disease control

1 Introduction

Nipah virus (NiV) disease is a deadly emerging contagious disease caused by Nipah virus that poses a growing concern to public health in Southeast Asia. It is caused by the zoonotic single-stranded RNA NiV, which is a member of the Henipavirus genus in the Paramyxoviridae family with subfamily Paramyxovirina [1]. Since its first recognized outbreak in Singapore and Malaysia in 1998-1999, NiV has caused recurrent outbreaks with substantial case fatality and significant socio-economic disruption [2–4]. Several hundred cases have been reported globally, and the reported case fatality has ranged from 40% to 75% in outbreaks since 2001. This underscores the necessity for a better understanding of the transmission dynamics and control of the disease [5].

Fruit bats are the primary natural reservoir of NiV, disseminating the virus in saliva, urine, semen, and excreta, and serving as the primary zoonotic source of human infection [6]. Evidence of NiV infection

in fruit bats has been reported throughout Southeast Asia [5, 7, 8], with serological evidence also documented outside the region [9–12] as well. Outbreaks of NiV disease in human populations show a strong seasonal pattern during spring and winter, which is likely connected with the date palm sap harvesting season [5] and the breeding season of Pteropus (flying foxes) bats. In addition to zoonotic spillover, human-to-human transmission occurs through close contact with infected individuals and exposure to respiratory secretions [5, 13–16]. Human-to-human transmission was particularly evident during outbreaks in Bangladesh and India, which accounted for approximately 51% and 75% of cases, respectively [17]. Reported incubation periods of NiV in many humans are commonly 4-14 days [2, 5], although longer delays have been documented [18].

Clinically, NiV infection ranges from asymptomatic or non-encephalitic illness to severe pneumonia and encephalitis [19]. Encephalitis, characterized by necrosis and vasculitis in the central nervous system (CNS), may present as either acute or late-onset. The latter can be difficult to diagnose since NiV exposure may have occurred several months earlier. Additionally, non-encephalitic infection with relapse and late-onset encephalitis reported several months after initial recovery [18, 20]. A study by Chattu et al. [17] confirmed that over 20 cases of relapsing NiV encephalitis have been observed, including one occurring 11 years after an asymptomatic infection. As of 2025, no licensed therapies or vaccines are available for NiV disease [5, 21]. Current treatment is limited to supportive care and symptom management; however, a vaccine is currently under development [22], and several antiviral drugs are under investigation, such as ribavirin, which has shown potential in reducing mortality in acute Nipah encephalitis [23]. To reduce transmission, avoidance of close contact with infected individuals, regular hand washing, and the use of protective equipment when caring for sick individuals are recommended [24].

In recent years, several mathematical studies have examined NiV transmission dynamics using compartmental models [25–30]. Biswas et al. [25] developed an SIR model with optimal control and showed that educational interventions discouraging consumption of raw date palm sap can reduce transmission. Mondal et al. [26] developed a model that includes quarantine and monitoring restrictions. They concluded that quarantine and improved hygiene can effectively control the spread of disease. Khan et al. [27] put out a model encompassing human-to-human and food-borne transmission, identifying improved treatment, diminished contact rates, and heightened vaccine efficacy as key drivers in eradication. Xie et al. [28] showed that time-varying interventions can work better than constant controls in lowering incidence. Tyagi et al. [30] introduced an asymptomatic class and examined equilibrium stability, determining that early-stage intervention can significantly diminish transmission.

However, despite the clinical documentation of relapse and delayed-onset encephalitis in Nipah virus infections, their population-level epidemiological consequences and interaction with biological time delays remain poorly understood due to limited clinical follow-up, underreporting, and logistical challenges associated in prolonged surveillance in high-risk areas. No study to date has explicitly integrated relapse rates, delayed-onset encephalitis, and incubation delays into a cohesive modeling framework for NiV disease. Relapse and delayed-onset encephalitis can reintegrate recovered persons into infectious compartments, perpetuating transmission or producing recurring epidemic waves, while incubation delay may influence the severity of outbreaks. Addressing this gap is important for understanding the complex transmission dynamics of NiV infection and for guiding effective disease control strategies.

In this study, we propose a delay differential equation (DDE) model for human-to-human NiV transmission, aimed at encapsulating essential temporal characteristics indicated by clinical and surveillance evidence. The model includes an incubation delay describing progression from exposure to infectiousness, a relapse pathway that returns recovered individuals to an asymptomatic stage, and a post-recovery delay reflecting delayed-onset encephalitis. Model parameters, including transmission rate, relapse rates, and time delays, are estimated from annual NiV incidence data from Bangladesh. We employ the model to examine whether relapse and post-recovery delay mechanisms can alter classical epidemic threshold results, and to evaluate whether biologically driven delays can generate delayed or recurring outbreak patterns. We characterize equilibria and their stability and study Hopf bifurcations and oscillatory dy-

namics induced by delays. Finally, numerical simulations and scenario-based sensitivity analyses quantify how relapse and each delay mechanism shape outbreak timing, peak magnitude, and post-peak dynamics across epidemiologically plausible regimes.

The rest of the paper is organized as follows. Section 2 delineates the model formulation, establishes positivity and boundedness of the solutions. Section 3 quantifies the contribution of relapse to infection dynamics. Section 4 presents the dynamical analysis, encompassing the computation of the primary transmission threshold (R_0), the stability of equilibria, and the examination of Hopf bifurcation. Section 5 describes parameter estimation and model fitting. Section 6 presents numerical simulations, sensitivity analyses, and illustrative bifurcation results. Finally, Section 7 discusses implications, limitations, and future research directions.

2 Model structure

In this study, we extend the framework of Tyagi et al. [30] to develop a compartmental model of NiV transmission in humans via direct contact, incorporating relapse rate and time delays associated with incubation and developing encephalitis. The total population (N) is divided into seven different compartments, representing the populations of susceptible (S), exposed (E), asymptomatic (I_1), symptomatic (I_2), hospitalized (H), under treatment (T), and recovered (R) individuals with $N = S+E_1+I_1+I_2+H+T+R$. The following system of equations and the schematic flow diagram in Figure 1 describe the proposed model with multiple time delays:

$$\begin{aligned}
\frac{dS}{dt} &= A - \mu S - \alpha S(I_1 + I_2),\\
\frac{dE}{dt} &= \alpha S(I_1 + I_2) - \alpha S(t-\omega_1)(I_1(t-\omega_1) + I_2(t-\omega_1))e^{-\mu\omega_1} - \mu E,\\
\frac{dI_1}{dt} &= \alpha S(t-\omega_1)(I_1(t-\omega_1) + I_2(t-\omega_1))e^{-\mu\omega_1} - (\tau_1 + \gamma + \mu)I_1 + \psi_1 R,\\
\frac{dI_2}{dt} &= \gamma I_1 - (\tau_2 + \xi + \mu + \delta)I_2 + \psi_2 R(t-\omega_2)e^{-\mu\omega_2},\\
\frac{dH}{dt} &= \xi I_2 - (\phi_H + \mu + \upsilon\delta)H,\\
\frac{dT}{dt} &= \tau_1 I_1 + \tau_2 I_2 - (\phi_T + \mu)T,\\
\frac{dR}{dt} &= \phi_H H + \phi_T T - \mu R - \psi_1 R - \psi_2 R(t-\omega_2)e^{-\mu\omega_2}.
\end{aligned} \tag{2.1}$$

In model (2.1), we assume that both asymptomatic and symptomatic individuals in I_1 and I_2, respectively, spread the disease at the same transmission rate α. We also consider that hospitalized individuals in H are less likely to die than infectious individuals in I_2 by using the parameter $0 < \upsilon \leq 1$, where $\upsilon = 1$ means that hospitalized individuals die at the same rate as infectious individuals in I_2, and the value closer to zero represents lower probability of dying. The parameter ψ_1 denotes the relapse rate, where recovered individuals in R go back to the asymptomatic compartment (I_1) [31,32]. The parameter ψ_2 represents the rate at which recovered individuals develop onset encephalitis and return to the symptomatic compartment I_2. The parameter ω_1 denotes the incubation delay, which indicates that after infection, an individual stays in the exposed compartment (E) for some time before moving to the asymptomatic compartment and the term $\alpha S(t-\omega_1)(I_1(t-\omega_1)+I_2(t-\omega_1))e^{-\mu\omega_1}$ represents the individuals surviving in the incubation period ω_1. Parameter ω_2 represents the time delay, corresponding to the time between recovery and subsequent onset of encephalitis and the term $\psi_2 R(t-\omega_2)e^{-\mu\omega_2}$ represents the individuals surviving in the period ω_2. The terms $e^{-\mu\omega_1}$ and $e^{-\mu\omega_2}$ represent the survival probabilities of individuals over the time delays ω_1 and ω_2, respectively, where μ is the mortality rate. The biological interpretation of the remaining parameters

in model (2.1) are summarized in Table 1.

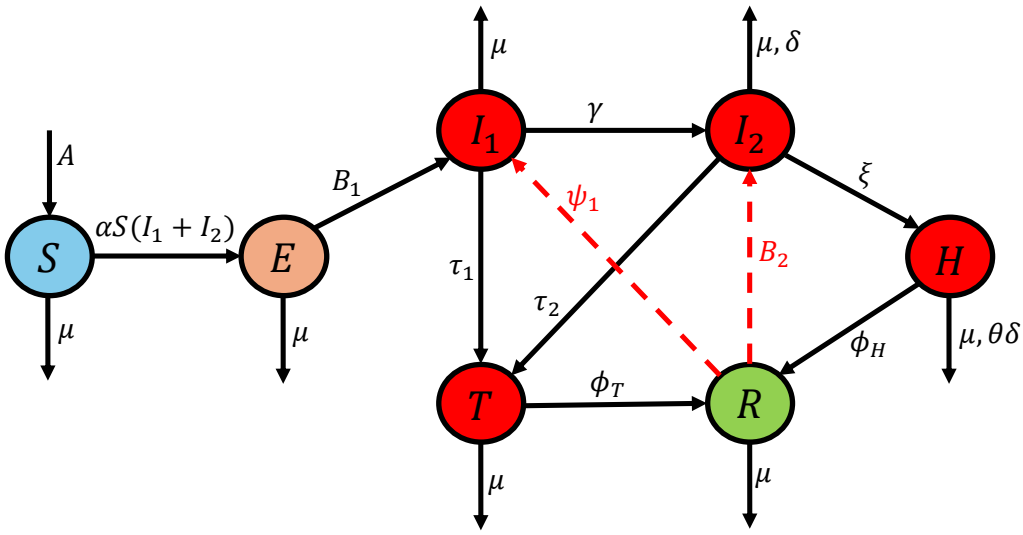

Figure 1: Schematic diagram illustrating the flow between the different compartments in the model (2.1), where $B_1 = \alpha S(t-\omega_1)(I_1(t-\omega_1)+I_2(t-\omega_1))e^{-\mu\omega_1}$ and $B_2 = \psi_2 R(t-\omega_2)e^{-\mu\omega_2}$.

To determine the solutions of model (2.1), we consider the following associated initial conditions

$$\begin{aligned} S(\theta) =& \Phi_1(\theta), E(\theta) = \Phi_2(\theta), I_1(\theta) = \Phi_3(\theta), I_2(\theta) = \Phi_4(\theta), \\ H(\theta) =& \Phi_5(\theta), T(\theta) = \Phi_6(\theta), R(\theta) = \Phi_7(\theta), \end{aligned} \tag{2.2}$$

where $\omega = \max\{\omega_1, \omega_2\}$, $\theta \in [-\omega, 0]$, $(\Phi_1(\theta), \Phi_2(\theta), \Phi_3(\theta), \Phi_4(\theta), \Phi_5(\theta), \Phi_6(\theta), \Phi_7(\theta)) \in C([-\omega, 0], \mathbb{R}^7)$, and $C([-\omega, 0], \mathbb{R}^7)$ is the Banach space of continuous functions from $[-\omega, 0]$ to $\mathbb{R}^7$. Since each population has non-negative values, we consider non-negative initial histories, i.e.

$$\Phi_i(\theta) \geq 0, \qquad \theta \in [-\omega, 0], \quad i = 1, \ldots, 7.$$

In addition, to ensure positivity of the solutions for the compartment E (and to preserve its biological cohort interpretation), the initial condition for E is defined in relation to the other variables as the following compatibility condition:

$$\Phi_2(0) = \int_{-\omega_1}^{0} \alpha \Phi_1(s)(\Phi_3(s) + \Phi_4(s))e^{\mu s}\, ds. \tag{2.3}$$

This compatibility condition is not required for local existence and uniqueness of solutions of the delay system, but it is imposed here to obtain the integral representation of E used in the positivity analysis. If this condition is not imposed, positivity of E is not immediate from a standard boundary argument.

For the R-equation in (2.1), due to the presence of the delayed loss term $-\psi_2 R(t-\omega_2)e^{-\mu\omega_2}$, an integral representation is not available; therefore positivity of R is not immediate from the same argument used for E. In the sequel we assume that along solutions of (2.1) satisfies

$$\phi_H H(t) + \phi_T T(t) \;\geq\; \psi_2 e^{-\mu\omega_2} R(t-\omega_2), \qquad t \geq 0. \tag{2.4}$$

This condition is sufficient to ensure that the recovered compartment remains non-negative.

From the fundamental theory of functional differential equations [35], model (2.1) with the initial conditions (2.2) possesses a unique local solution. Before examining the asymptotic properties of system (2.1), it is essential to first analyze positivity and boundedness of the solutions. We here outline the ensuing result for the biologically feasible region of system (2.1), and the proof is presented in Appendix A.

Theorem 2.1. *Assume non-negative initial histories and (2.4). The region*

$$\Psi = \Big\{(S(t), E(t), I_1(t), I_2(t), H(t), T(t), R(t)) \in \mathbb{R}^7_+ : S(t) + E(t) + I_1(t) + I_2(t) + H(t) + T(t) + R(t) \leq \frac{A}{\mu}, \text{ for all } t \geq 0\Big\} \tag{2.5}$$

is positively invariant with respect to the DDE system (2.1). Moreover, all nonnegative solutions of (2.1) are bounded, and satisfy

$$\limsup_{t\to\infty}\big(S(t) + E(t) + I_1(t) + I_2(t) + H(t) + T(t) + R(t)\big) \leq \frac{A}{\mu}.$$

Table 1: Biological description of the parameters in model (2.1).

Parameters	Biological interpretation	Numerical value (year^{-1})	Source	95% CI
A	Recruitment rate of individuals joining the susceptible compartment	$1.8595e+06$	$N(0) \times \mu$	-
μ	Natural death rate	1/73.57	[27]	-
α	Disease transmission rate	0.605e-07	Estimated	0.140e-07 - 0.722e-07
τ_1	Treatment rate of asymptomatic individuals	146	Assumed	-
γ	Progression rate from asymptomatic to symptomatic stage	45.625	[5]	-
ψ_1	Relapse rate	1.968	Estimated	1.375 - 3.992
τ_2	Treatment rate of symptomatic individuals	146	[27]	-
ξ	Hospitalization rate of symptomatic individuals	146	[27]	-
δ	Disease-induced death rate	10.733	Estimated	2.336 - 13.378
ψ_2	Rate at which recovered individuals develop onset encephalitis	2.612	Estimated	0.167 - 2.943
ϕ_H	Recovery rate of hospitalized individuals	32.85	[27]	-
υ	A coefficient accounts for reduced mortality in hospitalized (H) compared to infectious (I_2) individuals	0.4	Assumed	-
ϕ_T	Recovery rate of treated individuals	32.85	[27]	-
ω_1	Incubation delay	2.874	Estimated	2.205 - 4.426
ω_2	Time delay in developing onset encephalitis of recovered individuals	5.408	Estimated	2.326 - 7.686

3 Contribution of relapse to infection dynamics

To assess when relapse becomes an epidemiologically important mechanism shaping epidemic dynamics, we introduce two relapse contribution fractions derived from the model trajectories. The first compares the size

of the recovered population to the actively infectious population, reflecting the availability of individuals who may re-enter infectious states through relapse. The second quantifies the relative contribution of relapse-related returns to infectious compartments compared with incident infection arising from human-to-human transmission.

We define the population ratio at time t as the ratio of recovered individuals to the total infectious population,

$$\text{Pool ratio}(t) \;=\; \frac{R(t)}{I_1(t) + I_2(t)}. \tag{3.1}$$

Large values of pool ratio indicate that the recovered population substantially exceeds the number of currently infectious individuals. In this regime, relapse processes can make an increasingly important contribution to epidemic dynamics, particularly during the post-peak phase when susceptible-driven transmission has declined.

In the model, incident infection arising from human-to-human transmission enters the first infectious class after an incubation delay ω_1. The corresponding rate of appearance of newly infectious individuals is given by

$$F_{\text{infection}}(t) \;=\; \alpha\, e^{-\mu\omega_1}\, S(t-\omega_1)\,\big(I_1(t-\omega_1) + I_2(t-\omega_1)\big), \tag{3.2}$$

where the exponential term accounts for survival over the incubation period under natural mortality.

Relapse contributes to epidemic dynamics through two biologically distinct pathways. First, recovered individuals may return directly to the initial infectious class,

$$F_{\text{relapse},1}(t) \;=\; \psi_1\, R(t), \tag{3.3}$$

and second, relapse may occur after a delay ω_2, contributing to the second infectious class,

$$F_{\text{relapse},2}(t) \;=\; \psi_2\, e^{-\mu\omega_2}\, R(t-\omega_2). \tag{3.4}$$

We then define the relapse contribution fraction as the proportion of incident infectious individuals attributable to relapse-related processes,

$$\text{Relapse fraction}(t) \;=\; \frac{F_{\text{relapse},1}(t) + F_{\text{relapse},2}(t)}{F_{\text{infection}}(t) + F_{\text{relapse},1}(t) + F_{\text{relapse},2}(t)}. \tag{3.5}$$

Values of relapse fraction close to zero indicate that epidemic incidence is primarily shaped by human-to-human transmission, whereas larger values indicate that relapse-related returns to infectious states contribute substantially to observed disease burden. Although no sharp threshold separates primary transmission from relapse-driven dynamics, the relapse contribution fraction provides insight into when relapse becomes epidemiologically relevant. In particular, relapse tends to play a significant role once the recovered population substantially exceeds the infectious population, even under modest relapse rates. This behavior is further illustrated via numerical simulations.

4 Dynamical analysis

To determine the long-term dynamics of the disease, we compute the disease-free and endemic equilibria of system (2.1), together with their feasibility conditions, representing states in which the infection either vanishes or persists at a stable level. To characterize disease extinction or persistence, we first derive the critical thresholds in terms of the basic and effective reproduction numbers of the model. Next, we analyze the local stability of each equilibrium by linearizing the system around the corresponding equilibrium and examining the eigenvalues of the resulting Jacobian matrix. The analysis of the characteristic equations that are associated with the inclusion of time delays is necessary, as their roots determine the local stability properties of the equilibria. We identify parameter regimes in which all characteristic roots have negative

real parts, which suggests local asymptotic stability. Additionally, we emphasize instances in which a pair of purely imaginary roots arises. In particular, for the endemic equilibrium, the time-delay parameters (ω_1 and ω_2) are treated as bifurcation parameters, allowing us to determine critical threshold values beyond which the qualitative nature of the system's dynamics changes.

4.1 Disease-free equilibrium and primary-transmission threshold

The disease-free equilibrium (DFE) is characterized by the absence of infection, i.e., all infected compartments are set to zero. Since R depends on H and T, it also vanishes in this case. Substituting these conditions into system (2.1), the disease-free equilibrium (DFE) (denoted by D_0), is given by the following expression:

$$D_0 = \left(\frac{A}{\mu}, 0, 0, 0, 0, 0, 0\right).$$

We use the next generation matrix method [33, 34] to compute the primary-transmission threshold, denoted by R_0, which first requires the computation of two matrices, one that keeps track of new infection terms (denoted by f) and the other that tracks the linear transition terms (denoted by v). By considering $x = (I_1, I_2, H, T)^T$, we have

$$x' = f(x) - v(x),$$

where

$$f(x) = \begin{pmatrix} \alpha S(t-\omega_1)(I_1(t-\omega_1) + I_2(t-\omega_1))e^{-\mu\omega_1} \\ 0 \\ 0 \\ 0 \end{pmatrix},$$

and

$$v(x) = \begin{pmatrix} (\tau_1 + \gamma + \mu)I_1 - \psi_1 R \\ -\gamma I_1 + (\tau_2 + \xi + \mu + \delta)I_2 - \psi_2 R(t-\omega_2)e^{-\mu\omega_2} \\ -\xi I_2 + (\phi_H + \mu + \upsilon\delta)H \\ -\tau_1 I_1 - \tau_2 I_2 + (\phi_T + \mu)T \end{pmatrix}.$$

Further, the Jacobian matrices of $f(x)$ and $v(x)$ at D_0, denoted by F and V, are written as

$$F = Df(D_0) = \begin{pmatrix} \alpha\frac{A}{\mu}e^{-\mu\omega_1} & \alpha\frac{A}{\mu}e^{-\mu\omega_1} & 0 & 0 \\ 0 & 0 & 0 & 0 \\ 0 & 0 & 0 & 0 \\ 0 & 0 & 0 & 0 \end{pmatrix}$$

and

$$V = Dv(D_0) = \begin{pmatrix} (\tau_1 + \gamma + \mu) & 0 & 0 & 0 \\ -\gamma & (\tau_2 + \xi + \mu + \delta) & 0 & 0 \\ 0 & -\xi & (\phi_H + \mu + \upsilon\delta) & 0 \\ -\tau_1 & -\tau_2 & 0 & (\phi_T + \mu) \end{pmatrix}.$$

It is convenient to define the following quantity (where σ is the spectral radius):

$$R_0 = \sigma(FV^{-1}). \tag{4.1}$$

Hence, the primary-transmission threshold, R_0, is computed as

$$R_0 = \frac{\alpha A}{\mu}e^{-\mu\omega_1}\left[\frac{1}{(\tau_1 + \gamma + \mu)} + \frac{\gamma}{(\tau_1 + \gamma + \mu)(\tau_2 + \xi + \mu + \delta)}\right], \tag{4.2}$$

where, $\frac{A}{\mu}$ is the susceptible population at the disease-free equilibrium, $\frac{\alpha A}{\mu}$ is the disease transmission rate in the susceptible population at the disease-free equilibrium. The factor $e^{-\mu\omega_1}$ is the survival probability of the individuals through the incubation period ω_1. The quantity $\frac{1}{(\tau_1+\gamma+\mu)}$ is the average time in the asymptomatic class I_1. Moreover, $\frac{\gamma}{(\tau_1+\gamma+\mu)}$ is the probability of leaving I_1 by progressing to I_2 and $\frac{1}{(\tau_2+\xi+\mu+\delta)}$ is the average time of the infectious class I_2. Hence, the obtained R_0 represents the expected number of secondary infections generated by a typical infectious individual introduced into a wholly susceptible population.

4.2 Stability of disease-free equilibrium

Although the primary-transmission threshold R_0 provides a useful threshold for the primary transmission pathway, it does not fully capture the delayed relapse feedback generated by the recovered class in system (2.1). In particular, when $\psi_1, \psi_2 > 0$, recovered individuals may re-enter the infectious compartments and contribute to transmission through additional delayed loops, so local stability of the disease-free equilibrium cannot, in general, be characterized by R_0 alone. For this reason, we determine the local stability of D_0 by analyzing the characteristic roots of the full linearized delay system. The following theorem gives the exact local criterion for asymptotic (and exponential) stability of D_0, formulated in terms of the characteristic roots of the full linearized delay system for fixed $\omega_1, \omega_2 \geq 0$.

Theorem 4.1. *Let $\omega = \max\{\omega_1, \omega_2\}$, and let*

$$\det\big(\lambda I - A_0 - A_1 e^{-\lambda\omega_1} - A_2 e^{-\lambda\omega_2}\big) = 0$$

denote the characteristic equation of the linearization of (2.1) at D_0. If every characteristic root satisfies $\Re(\lambda) < 0$, then D_0 is locally asymptotically stable. Moreover, if there exists $\eta > 0$ such that all characteristic roots satisfy $\Re(\lambda) \leq -\eta$, then D_0 is locally exponentially stable.

Proof. Set $u(t) = \big(S(t) - A/\mu,\ E(t),\ I_1(t),\ I_2(t),\ H(t),\ T(t),\ R(t)\big)^\top$. In a neighborhood of D_0, system (2.1) defines a retarded functional differential equation on $C([-\omega, 0], \mathbb{R}^7)$ of the form

$$u'(t) = \mathcal{L}(u_t) + \mathcal{N}(u_t),$$

where $\mathcal{L}$ is the Fréchet derivative at D_0, and $\mathcal{N}(\varphi) = o(\|\varphi\|)$ as $\|\varphi\| \to 0$.

To determine the local stability of D_0, it suffices to consider the infection-feedback block

$$x(t) = \big(I_1(t), I_2(t), H(t), T(t), R(t)\big)^\top,$$

which satisfies the linear delay system

$$x'(t) = A_0 x(t) + A_1 x(t-\omega_1) + A_2 x(t-\omega_2), \tag{4.3}$$

with

$$A_0 = \begin{pmatrix} -(\tau_1+\gamma+\mu) & 0 & 0 & 0 & \psi_1 \\ \gamma & -(\tau_2+\xi+\mu+\delta) & 0 & 0 & 0 \\ 0 & \xi & -(\phi_H+\mu+\upsilon\delta) & 0 & 0 \\ \tau_1 & \tau_2 & 0 & -(\phi_T+\mu) & 0 \\ 0 & 0 & \phi_H & \phi_T & -(\mu+\psi_1) \end{pmatrix},$$

$$A_1 = \begin{pmatrix} \alpha\frac{A}{\mu}e^{-\mu\omega_1} & \alpha\frac{A}{\mu}e^{-\mu\omega_1} & 0 & 0 & 0 \\ 0 & 0 & 0 & 0 & 0 \\ 0 & 0 & 0 & 0 & 0 \\ 0 & 0 & 0 & 0 & 0 \\ 0 & 0 & 0 & 0 & 0 \end{pmatrix}, \qquad A_2 = \begin{pmatrix} 0 & 0 & 0 & 0 & 0 \\ 0 & 0 & 0 & 0 & \psi_2 e^{-\mu\omega_2} \\ 0 & 0 & 0 & 0 & 0 \\ 0 & 0 & 0 & 0 & 0 \\ 0 & 0 & 0 & 0 & -\psi_2 e^{-\mu\omega_2} \end{pmatrix}.$$

Seeking solutions of the form $x(t) = ve^{\lambda t}$ $(v \neq 0)$ yields the characteristic matrix

$$\Delta(\lambda) = \lambda I - A_0 - A_1 e^{-\lambda\omega_1} - A_2 e^{-\lambda\omega_2},$$

and hence the characteristic equation

$$\det\big(\lambda I - A_0 - A_1 e^{-\lambda\omega_1} - A_2 e^{-\lambda\omega_2}\big) = 0. \tag{4.4}$$

The $(S - A/\mu, E)$-subsystem is triangular and linearly stable when decoupled, with forcing terms depending on I_1, I_2. Hence it does not generate additional unstable spectrum beyond that of the infection-feedback block. Therefore, the spectral condition on (4.4) determines the local stability of the full linearization at D_0.

By the linear theory of retarded functional differential equations [35], if all characteristic roots satisfy $\Re(\lambda) < 0$, then the linearized system is asymptotically stable; if, in addition, the spectrum is bounded away from the imaginary axis, then the linearized system is exponentially stable. Finally, by the principle of linearized stability for retarded functional differential equations [35], the nonlinear equilibrium D_0 is locally asymptotically stable (respectively locally exponentially stable). □

From an epidemiological perspective, Theorem 4.1 shows that incubation and post-recovery delays do not, by themselves, destabilize the infection-free state, provided that the characteristic roots of the full linearized delay system remain in the left half-plane. In other words, delayed incubation and relapse pathways alone are insufficient to generate sustained transmission near the disease-free equilibrium in the absence of net growth of infection perturbations. At the same time, local asymptotic stability of the disease-free equilibrium is a local property and does not, by itself, imply global disease elimination. In particular, relapse may introduce additional feedback mechanisms through the recovered class that substantially modify persistence dynamics away from the disease-free state. As shown in the subsequent analysis, these relapse feedback effects can shift the effective persistence threshold away from the classical primary-transmission threshold $R_0 = 1$.

4.3 Existence and stability of endemic equilibrium

The endemic equilibrium (denoted by D^*) is given by the following expression:

$$D^* = (S^*, E^*, I_1^*, I_2^*, H^*, T^*, R^*),$$

which is obtained by setting all right-hand sides of system (2.1) equal to zero and solving the resulting algebraic system. This yields the following expressions:

$$\begin{aligned}
S^* =& \frac{(\tau_1 + \gamma + \mu) - \psi_1(r_1 + r_2 q)}{\alpha e^{-\mu\omega_1}(1+q)}, \quad E^* = \frac{(A - \mu S^*)(1 - e^{-\mu\omega_1})}{\mu}, \\
I_1^* =& \frac{A - \mu S^*}{\alpha S^*(1+q)}, \quad I_2^* = qI_1^*, \quad H^* = \frac{\xi}{\phi_H + \mu + \upsilon\delta} I_2^*, \\
T^* =& \frac{\tau_1 I_1^* + \tau_2 I_2^*}{\phi_T + \mu}, \quad R^* = r_1 I_1^* + r_2 I_2^*,
\end{aligned}$$

where

$$\begin{aligned}
q =& \frac{\gamma + \psi_2 r_1 e^{-\mu\omega_2}}{(\tau_2 + \xi + \mu + \delta) - \psi_2 r_2 e^{-\mu\omega_2}}, \quad r_1 = \frac{\phi_T \tau_1}{(\phi_T + \mu)(\mu + \psi_1 + \psi_2 e^{-\mu\omega_2})}, \\
r_2 =& \frac{\phi_T \tau_2}{(\phi_T + \mu)(\mu + \psi_1 + \psi_2 e^{-\mu\omega_2})} + \frac{\phi_H \xi}{(\phi_H + \mu + \upsilon\delta)(\mu + \psi_1 + \psi_2 e^{-\mu\omega_2})}.
\end{aligned}$$

Consequently, a biologically feasible endemic equilibrium is obtained provided

$$(\tau_2+\xi+\mu+\delta)-\psi_2 r_2 e^{-\mu\omega_2}>0, \qquad (\tau_1+\gamma+\mu)-\psi_1(r_1+r_2 q)>0, \qquad A-\mu S^*>0.$$

Reduction to the classical threshold in the absence of relapse: If $\psi_1=\psi_2=0$, we have $\mu+\psi_1+\psi_2 e^{-\mu\omega_2}=\mu$, and the relapse terms disappear from the expressions for q, r_1, and r_2. In particular,

$$q=\frac{\gamma}{(\tau_2+\xi+\mu+\delta)}, \qquad S^*=\frac{(\tau_1+\gamma+\mu)}{\alpha e^{-\mu\omega_1}(1+q)}=\frac{(\tau_1+\gamma+\mu)(\tau_2+\xi+\mu+\delta)}{\alpha e^{-\mu\omega_1}(\tau_2+\xi+\mu+\delta+\gamma)}.$$

The positivity condition $I_1^*>0$ is equivalent to $A-\mu S^*>0$, i.e.

$$\frac{A}{\mu S^*}>1.$$

Using the expression for S^*, we obtain

$$\begin{aligned}\frac{A}{\mu S^*} =& \frac{\alpha A}{\mu} e^{-\mu\omega_1}\frac{\tau_2+\xi+\mu+\delta+\gamma}{(\tau_1+\gamma+\mu)(\tau_2+\xi+\mu+\delta)}\\ =& \frac{\alpha A}{\mu} e^{-\mu\omega_1}\left(\frac{1}{(\tau_1+\gamma+\mu)}+\frac{\gamma}{(\tau_1+\gamma+\mu)(\tau_2+\xi+\mu+\delta)}\right)=R_0.\end{aligned}$$

Hence $A-\mu S^*>0$ is equivalent to $R_0>1$, and the endemic equilibrium condition reduces to the classical threshold $R_0>1$.

For $\psi_1,\psi_2>0$, the endemic equilibrium depends on relapse feedback through $\mu+\psi_1+\psi_2 e^{-\mu\omega_2}$, r_1, r_2, and q. Consequently, the existence of a positive endemic equilibrium is not determined by the primary-transmission threshold R_0 alone. In particular, relapse-induced feedback may shift the classical persistence threshold associated with $R_0=1$.

To analyze the local asymptotic stability of D^* for different cases of time delays, ω_1 and ω_2, we obtain the following results:

Theorem 4.2. *The endemic equilibrium D^* is locally asymptotically stable in the absence of time delays, i.e., for $\omega_1=\omega_2=0$.*

Theorem 4.3. *Under conditions H1 and H2, the endemic equilibrium D^* remains locally asymptotically stable for $\omega_1\in[0,\omega_1')$. Moreover, when $\omega_1=\omega_1'$, a family of periodic solutions bifurcates from D^* and system (2.1) undergoes a Hopf bifurcation.*

Theorem 4.4. *Under conditions H3 and H4, the endemic equilibrium D^* is locally asymptotically stable for $\omega_2\in[0,\omega_2')$. In addition, when $\omega_2=\omega_2'$, a family of periodic solutions bifurcates from D^* and system (2.1) undergoes a Hopf bifurcation.*

Theorem 4.5. *Under conditions H5 and H6, the endemic equilibrium D^* is locally asymptotically stable for $\omega_1\in[0,\omega_{11}')$, when ω_2 is fixed in its stable interval. Furthermore, when $\omega_1=\omega_{11}'$, system (2.1) undergoes a Hopf bifurcation at D^*, giving rise to a family of periodic solutions.*

Theorems 4.2-4.5 establish that the endemic equilibrium is locally asymptotically stable provided that the incubation delay and the delay in encephalitis development remain below their respective critical threshold values. The technical conditions H1-H6, which guarantee the existence of these critical delay thresholds, are introduced within the proofs and are presented in Appendix B. When these thresholds are exceeded, the endemic equilibrium loses stability through delay-induced mechanisms, which are examined in detail in the subsequent Hopf bifurcation analysis.

4.4 Properties of Hopf bifurcation

In the previous section, we investigated that a family of periodic solutions bifurcates from the endemic equilibrium, D^*, for distinct threshold values of the time-delay parameters, ω_1 and ω_2, in system (2.1). Here, we analyze the properties of Hopf bifurcation, particularly the direction and stability of Hopf bifurcation, at the threshold value of the time delay $\omega_1 = \omega'_{11}$. For this, we utilize the center manifold theorem and normal form theory [36]. Throughout the analysis, it is assumed that $\omega'_{22} < \omega'_{11}$, where $\omega'_{22} \in (0, \omega'_2)$.

Assume $\tilde{p}_1 = S - S^*, \tilde{p}_2 = E - E^*, \tilde{p}_3 = I_1 - I_1^*, \tilde{p}_4 = I_2 - I_2^*, \tilde{p}_5 = H - H^*, \tilde{p}_6 = T - T^*, \tilde{p}_7 = R - R^*$ and $\omega_1 = \zeta + \omega'_{11}$, where $\zeta \in \mathbb{R}$. Further, normalize the time delay ω_1 by scaling time t as $t \to t/\omega_1$. Thus, system (2.1) attains the following functional differential form:

$$\dot{\tilde{p}}(t) = F(\zeta, \tilde{p}_t) + L_\zeta(\tilde{p}_t). \tag{4.5}$$

Using similar notations as in Hassard et al. [36], the detailed derivation of the corresponding linear operator formulation, adjoint system, bilinear inner form, eigenvectors, center manifold reduction, and normal form coefficients is presented in Appendix B. In particular, we determine

$$\begin{aligned}
c_1(0) &= \frac{i}{2\omega'_{11}p'}\left(g_{20}g_{11} - 2|g_{11}|^2 - \frac{|g_{02}|^2}{3}\right) + \frac{g_{21}}{2}, \\
\mu_2 &= -\frac{\Re\{c_1(0)\}}{\Re\{\lambda'(\omega'_{11})\}}, \\
\beta_2 &= 2\Re\{c_1(0)\}, \\
T_2 &= -\frac{\Im\{c_1(0)\} + \mu_2\Im\{\lambda'(\omega'_{11})\}}{\omega'_{11}p'}.
\end{aligned}$$

The above terms determine the behavior of bifurcating periodic solutions at the threshold value of the time delay $\omega_1 = \omega'_{11}$. In particular, μ_2 governs the direction of Hopf bifurcation: if $\mu_2 > 0$ ($\mu_2 < 0$), then the Hopf bifurcation is supercritical (subcritical) and the bifurcating periodic solution exists for $\omega_1 > \omega'_{11}$ ($\omega_1 < \omega'_{11}$). β_2 governs the stability of the bifurcating periodic solution: the bifurcating periodic solution is stable (unstable) if $\beta_2 < 0$ ($\beta_2 > 0$). T_2 determines the period of the bifurcating periodic solution: if $T_2 > 0$, the period increases; otherwise, it decreases.

4.5 Estimation of the length of time delays to sustain stability

This section determines the length of time delays that sustain the stability of system (2.1) by utilizing the Nyquist criterion [38]. To prove this, system (2.1) and the space of all real-valued continuous functions are considered on $[-\omega, +\infty)$ with the initial conditions provided earlier. Using the ensuing transformations $S = S^* + \tilde{p}_1, E = E^* + \tilde{p}_2, I_1 = I_1^* + \tilde{p}_3, I_2 = I_2^* + \tilde{p}_4, H = H^* + \tilde{p}_5, T = T^* + \tilde{p}_6, R = R^* + \tilde{p}_7$, we obtain the linearized system and the corresponding characteristic equation (see Appendix B for the detailed derivation). Local stability of D^* follows if

$$\Re(\Xi(i\eta_0)) = 0, \tag{4.6}$$

$$\Im(\Xi(i\eta_0)) > 0, \tag{4.7}$$

where η_0 is the smallest positive root of Eq. (4.6).

Theorem 4.2 shows that D^* is locally stable when $\omega_1 = \omega_2 = 0$. Hence, by continuity, all eigenvalues have negative real parts for sufficiently small $\omega_1 > 0, \omega_2 > 0$, provided that as ω_1 and ω_2 increase from zero, no eigenvalues with positive real parts bifurcate from infinity. This can be verified by Butler's lemma [39]. We next consider the case $\omega_1 > 0$ and ω_2 in its stable interval, as in Theorem 4.5. If the resulting inequalities (derived in Appendix B) are satisfied simultaneously, then these conditions are sufficient to guarantee stability. We will utilize these to obtain an estimation of the length of the time delay. Our main

aim is to find an upper bound η^+ on η_0 independent of ω_1 and ω_2, and then estimate ω_1 so that Eq. (4.7) is satisfied for all values of η, $0 \leq \eta \leq \eta^+$, and hence in particular at $\eta = \eta_0$.

Consequently, we obtain

$$2\sin^2\left(\frac{\eta_0\omega_1}{2}\right)\tilde{K}_{11}(\eta_0) + \sin(\eta_0\omega_1)\tilde{K}_{12}(\eta_0) \leq \tilde{K}_{13}(\eta_0), \tag{4.8}$$

where $\tilde{K}_{11}(\eta_0)$, $\tilde{K}_{12}(\eta_0)$, and $\tilde{K}_{13}(\eta_0)$ are given in Appendix B. Now, from inequality (4.8), we have

$$\tilde{K}_{11}(\eta^+)\omega_1^2 + \tilde{K}_{12}(\eta^+)\omega_1 \leq \tilde{K}_{13}(\eta^+), \tag{4.9}$$

where $\tilde{K}_{11}(\eta^+) = \frac{\eta^{+2}}{2}\left|\tilde{K}_{11}(\eta_0)\right|_{\eta_0=\eta^+}$, $\tilde{K}_{12}(\eta^+) = \eta^+\left|\tilde{K}_{12}(\eta_0)\right|_{\eta_0=\eta^+}$, and $\tilde{K}_{13}(\eta^+) = \left(\tilde{K}_{13}(\eta_0)\right)_{\eta_0=\eta^+}$. Hence, if

$$\omega_1^+ = \frac{1}{2\tilde{K}_{11}(\eta^+)}\left(-\tilde{K}_{12}(\eta^+) + \sqrt{\tilde{K}_{12}^2(\eta^+) + 4\tilde{K}_{11}(\eta^+)\tilde{K}_{13}(\eta^+)}\right), \tag{4.10}$$

then stability is preserved for $0 \leq \omega_1 < \omega_1^+$.

A similar procedure can be followed to compute the length of the time delay ω_2 for which stability is sustained, considering ω_1 in its stable interval.

5 Model fitting to NiV incidence data

We use NiV incidence data from Bangladesh as the primary dataset for model fitting and parameter estimation. The dataset consists of yearly case counts from 2001 to 2024, reported across the country and collected from the official website of the Institute of Epidemiology, Disease Control and Research (IEDCR), Bangladesh [40]. These yearly cases (Table 2) serve as the empirical basis for model fitting and the estimation of key epidemiological parameters including transmission rate, relapse rate and time delays.

Table 2: Number of NiV cases per year (incidence) in Bangladesh from 2001 to 2024 adopted from [40].

Year	2001	2002	2003	2004	2005	2006	2007	2008	2009	2010	2011	2012
Cases	13	0	12	67	12	0	18	11	4	18	43	17
Year	2013	2014	2015	2016	2017	2018	2019	2020	2021	2022	2023	2024
Cases	31	37	15	0	3	4	8	7	2	3	13	5

The model (2.1) has multiple parameters, with values for at least nine of them available from the NiV disease literature, which are provided in Table 1. The value of recruitment rate (A) is obtained from the fraction A/μ at disease-free equilibrium, i.e., prior to the emergence of the NiV disease. Since the total population of Bangladesh in 2001 was 136,805,810 [41] and $1/\mu$ is the individual average life span (73.57 years [27]), then $A =$ total population $\times\mu = 1.8595e + 06$ per year. According to the World Health Organization (WHO), the progression time to become symptomatic from the asymptomatic stage is 4-14 days, so we consider an average progression time of 8 days. The progression rate (γ) from the asymptomatic stage to the symptomatic stage is $\gamma = 365/8 = 45.625$ per year. According to Khan et al. [27], the treatment rate is 0.4 per day (average 2.5 days), therefore, the treatment rates for both asymptomatic and symptomatic individuals are $\tau_1 = \tau_2 = 0.4 \times 365 = 146$ per year. We also set the hospitalization rate of symptomatic individuals to be $\xi = 146$ per year. We consider recovery time approximately to be 11.11 days [27], which follows the recovery rate of both symptomatic and hospitalized individuals to be $365/11.11 = 32.85$ per year.

At the beginning of the simulation, the initial values of the system's state variables are either obtained from the literature or assumed, except for the exposed individuals $E(0)$. The total population at the initial of the NiV disease outbreak ($N(0)$) is the total population size of Bangladesh in 2001 (136,805,810). The

initial value of the susceptible population is $S(0) = N(0) - E(0) - I_1(0)$. We assume that the initial values of asymptomatic and symptomatic individuals are $I_1(0) = I_2(0) = 3$. Further, we assume the initial value of hospitalized individuals (H) to be $H(0) = 1$ and under treatment (T) to be $T(0) = 2$. The number of recovered individuals is set as zero at the initial of the outbreak, i.e., $R(0) = 0$.

We estimate the model parameters by solving a least-squares minimization problem using MATLAB's built-in *lsqcurvefit* function [42], which supports parameter estimation within bounded ranges. We select six parameters for estimation including transmission rate (α), relapse rates (ψ_1 and ψ_2), disease induced death rate (δ), incubation delay (ω_1), and time delay in developing encephalitis (ω_2). In addition, some of the state variable's initial conditions are estimated as well. We also obtain 95% confidence interval (CI) for the estimated parameters considering the bootstrap procedure and 1000 bootstrap samples. Additionally, we generate a five-year prediction for NiV cases in Bangladesh using the calibrated model. The objective function to be minimized is the Root Mean Square Error (RMSE), which is generally used as a metric to measure the difference between data and the model output, defined by

$$RMSE = \sqrt{\frac{1}{n}\sum_{i=1}^{n}(Y_i - \hat{Y}_i)^2}, \quad i = 1, 2, \ldots, n, \tag{5.1}$$

where Y_i represents the vector of yearly cases of NiV within the period of consideration of length n, while $\hat{Y}_i$ is the corresponding model output. We also verified the goodness of fit results by computing the residuals, defined as

$$Residuals = \{Y_i - \hat{Y}_i | i = 1, 2, \ldots, n\}. \tag{5.2}$$

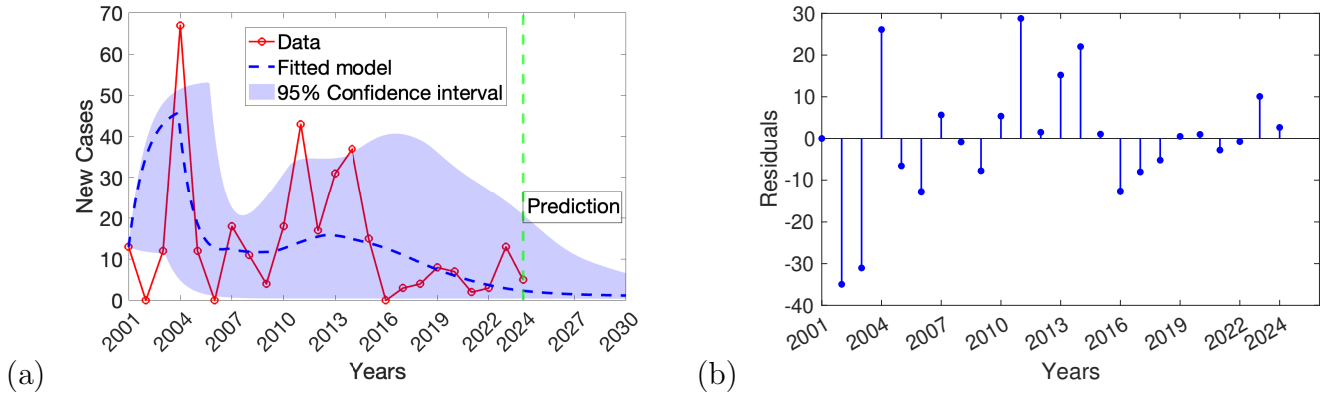

Figure 2: Data fitting of the model (2.1) using year-wise cases of NiV disease in Bangladesh from 2001 to 2024. (a) Least-squares fitting of the model (2.1), depicting the new cases per year generated by the model (blue curve), compared to the cases of NiV disease per year in Bangladesh (red circles), obtained from [40]. Blue shaded region illustrates the 95% confidence interval (CI). (b) Residuals of the data fitting.

The model fitting to NiV incidence data from Bangladesh shows that the fitted curve closely follows the observed trend, with a RMSE of 14.599 (Figure 2(a)). This error reflects the irregularity and variability of the annual case counts, which range from 0 to 67. The abrupt fluctuations in the data cannot be precisely replicated by epidemic models based on conventional differential equations, as they generate smooth trajectories. Consequently, the RMSE should be considered in the context of the data's dispersion. Nevertheless, the model effectively captures the overall dynamics of the epidemic, despite its inability to match every irregular point. The five-year forecast suggests that NiV cases will continue to be present in Bangladesh until 2030. The residuals are randomly distributed and small, suggesting a reasonably good fit (Figure 2(b)). The estimated initial number of exposed individuals $E(0)$ is 37.988 (95% CI: 2.370 - 96.434) based on the data fitting. Other parameters' estimated values are presented in Table 1.

6 Numerical simulation

To explore the epidemic dynamics of NiV under varying relapse rates and time delays, we conduct a series of numerical simulations across alternative epidemiological scenarios, including different levels of transmission intensity and treatment-associated rates. Numerical solutions of system (2.1) are obtained using MATLAB's built-in delay differential equation solver `dde23`, which is well suited for systems with time delays [42, 43]. All simulations are initialized using the baseline parameter values reported in Table 1. To examine the sensitivity of epidemic outcomes to key mechanisms, we systematically vary model parameters around their baseline values, while holding all remaining parameters fixed. This approach allows us to evaluate how plausible changes in relapse rate, time delays, transmission rate, and treatment-related parameters influence epidemic trajectories under alternative scenarios. These visualizations provide a comparative overview of how combined parameter changes shape epidemic outcomes and highlight regions of heightened or reduced disease burden.

6.1 Impact of relapse and biological time delays on long-term NiV incidence

To examine how relapse and time delays shape epidemic trajectories, we vary the relapse rate (ψ_1), incubation delay (ω_1), and time delay in encephalitis development after recovery (ω_2) by ±10%, ±20%, and ±30% around their baseline estimated values, while holding all other parameters fixed. Model outputs are evaluated using time-series dynamics and cumulative incidence over the study period (2001 - 2030).

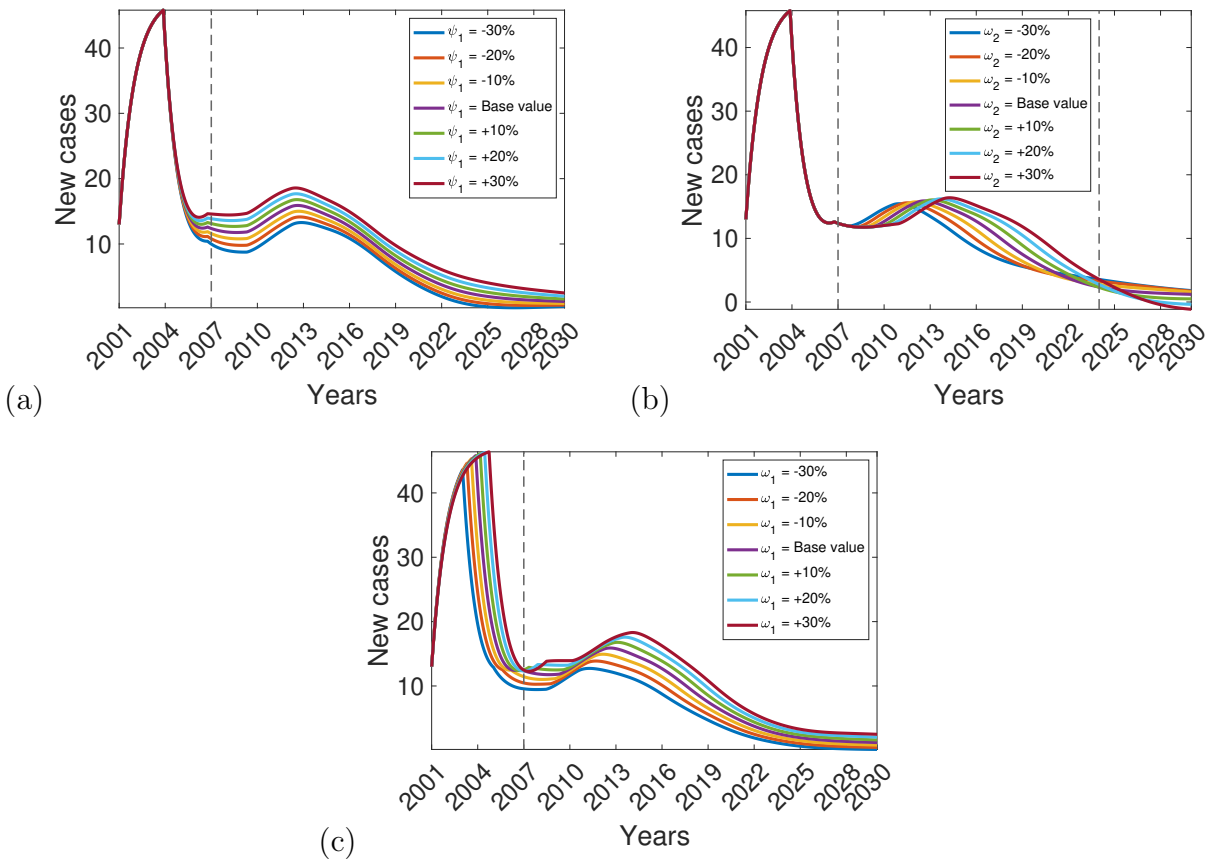

Figure 3: Time-series sensitivity analysis of NiV incidence (2001 - 2030) under variations in the (a) relapse rate (ψ_1), (b) time delay in encephalitis development (ω_2), and (c) incubation delay (ω_1). Each parameter is varied by ±10%, ±20%, and ±30% relative to baseline values, with all other parameters held fixed. Vertical dashed lines indicate the post-2007 period, corresponding to the secondary phase of the outbreak.

Time-series simulations reveal distinct roles for relapse and delay mechanisms in shaping NiV incidence

(Figure 3). Variations in the relapse rate (ψ_1) produces little changes during initial outbreak (2001-2007) but leads to progressively larger differences during the later phase of the outbreak, visible as a second hump or extended tail in the epidemic trajectory. Increasing values of ψ_1 increase new cases post-2007 period including the hump size of the outbreak, indicating that relapse sustains the disease burden for long time. Reductions in ψ_1 substantially suppress secondary peaks and accelerate convergence toward low-incidence dynamics. ω_2 exhibits a comparable pattern, with its influence becoming evident only after recovery has taken place, resulting in significant changes to the timing and magnitude of the secondary hump, while the early dynamics remain largely unaffected. In particular, higher values of ω_2 leads in delaying peak time of the later phase of the outbreak, but reducing the cases after 2024, reflecting the delayed return of recovered individuals to infectious states. In contrast, changes in incubation delay (ω_1) affect both the height and timing of the first peak of the outbreak as well as subsequent dynamics, reflecting its direct control over the progression from exposure to infectiousness. Collectively, these findings demonstrate that the primary factor influencing early epidemic growth is incubation delay (ω_1), while relapse dynamics are crucial in determining post-peak epidemic behavior. In particular, the significance of incorporating relapse into long-term control strategies is underscored by the fact that high relapse rates impede the rapid extinction of the disease.

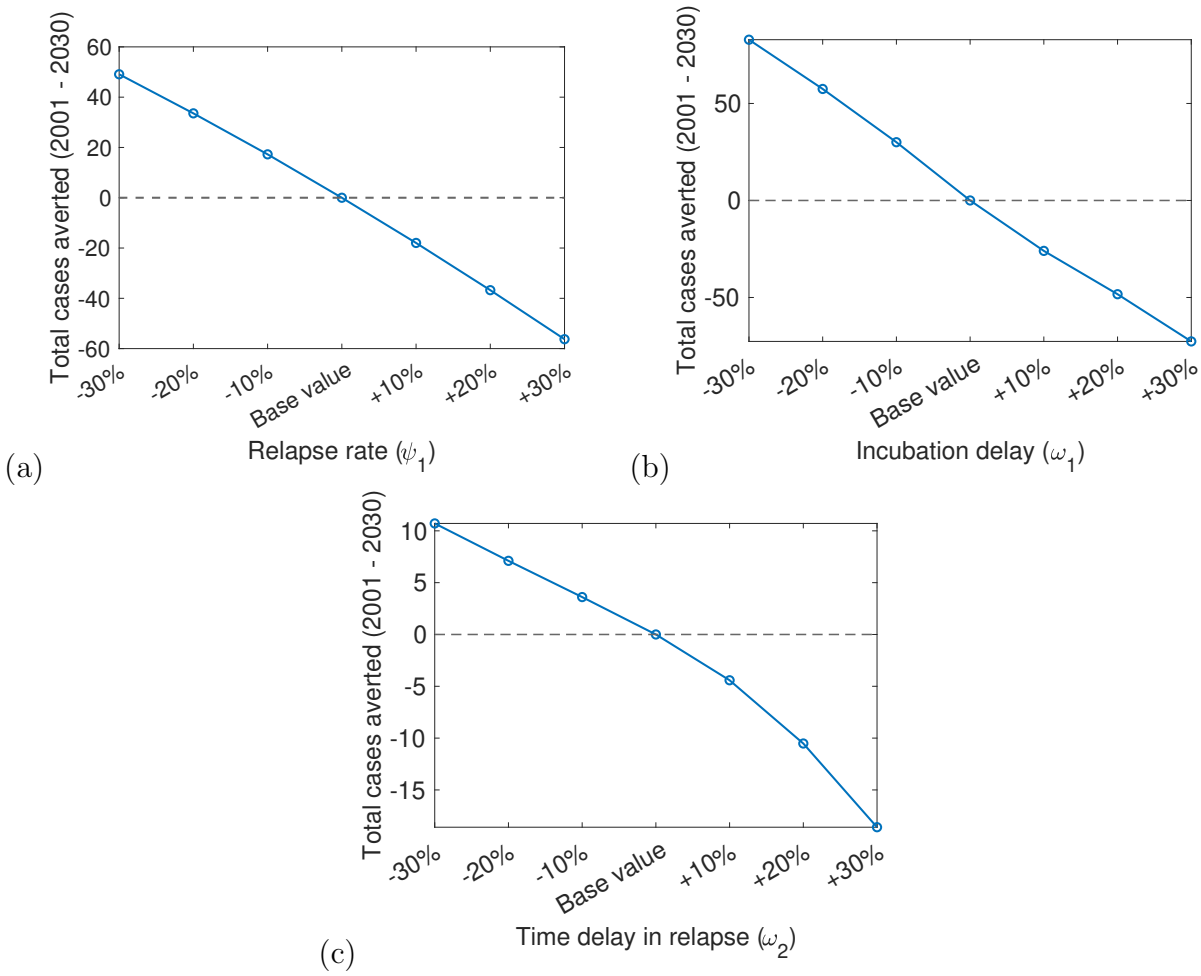

Figure 4: Total NiV cases averted over 2001 - 2030 under variations in key epidemiological parameters. Panels show the cumulative number of cases averted relative to the baseline scenario as a function of (a) relapse rate (ψ_1), (b) incubation delay (ω_1), and (c) time delay in encephalitis development (ω_2). Positive values indicate cases averted, while negative values indicate additional cases relative to baseline.

To quantify the long-term epidemiological impact of relapse and biological time delays, we computed the total number of NiV cases averted over the entire simulation period (2001-2030) relative to the base-

line scenario. Reductions in the incubation delay (ω_1) produce the largest decreases in total cases over 2001-2030, with a 30% reduction yielding a decrease of 23.29% ($\approx$ 83 cumulative cases averted) relative to baseline (Figure 4). Even moderate reductions of 10% and 20% result in substantial reductions in cumulative incidence of 16.15% and 8.44%, respectively, whereas increases in ω_1 produce a monotonic rise in total infections, highlighting the importance of early case detection and prompt clinical presentation. Changes in the relapse rate ψ_1 also exert a strong and monotonic effect on long-term disease burden. Over the model projection window, a 30% reduction in ψ_1 decreases total cases by approximately 14%, whereas increases in ψ_1 lead to higher cumulative incidence, indicating that relapse plays a dominant role in sustaining long-term transmission. These findings suggest that epidemic persistence is significantly influenced by relapse frequency in the presence of transmission conditions that remain unaltered.

By comparison, variations in the time delay in encephalitis development (ω_2) result relatively minor changes in cumulative incidence. A 30% decrease in ω_2 leads to a 3% reduction in total cases, while increases in ω_2 result in moderate increases in overall disease burden. In conjunction, these results indicate a distinct hierarchy of epidemiological influence, with the effective incubation delay (ω_1) having the most significant impact on cumulative incidence, followed by the relapse rate (ψ_1) and the encephalitis development delay (ω_2). For completeness, absolute cumulative case counts under each parameter scenario are provided in Appendix C (Figure 10, Tables 3, 4, and 5).

Figure 5 illustrates the time-dependent relapse-driven replenishment fraction, defined as the proportion of total inflow into infectious compartments attributable to relapse (i.e., the relapse inflow divided by the total inflow into infectious states). Early in the epidemic, most entries into infectious compartments arise from human-to-human transmission following incubation, and the contribution of relapse is limited. As the epidemic progresses and the recovered (clinically resolved) compartment accumulates, the contribution of relapse increases steadily. After the primary outbreak peak, the relapse fraction exceeds 80-90% under baseline transmission conditions, indicating that most entries into infectious states arise from relapse rather than from newly generated infections. The magnitude and timing of this shift depend on the human-to-human transmission rate. Under higher transmission intensity, new infections continue to contribute a substantial share of infectious inflow after the first peak, leading to lower and more temporally variable relapse fraction. In contrast, under weaker transmission, new infections become rare while the recovered pool continues to grow, so relapse rapidly becomes the dominant source of infectious-state replenishment. Mechanistically, this pattern reflects the increasing availability of a recovered reservoir that can re-enter infectious compartments through relapse particualrly during later epidemic phases.

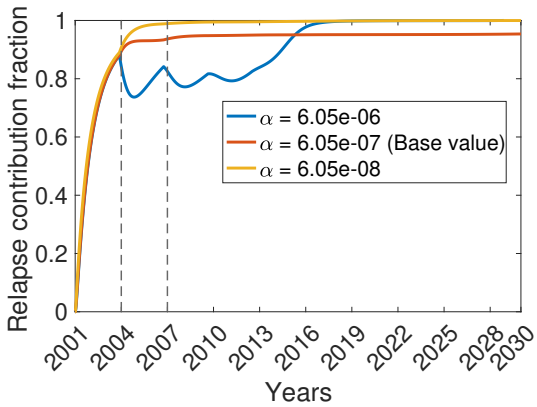

Figure 5: Time-varying contribution of relapse to the infectious population. The relapse-driven replenishment fraction represents the proportion of entries into infectious compartments attributable to relapse processes over time. The vertical dashed lines indicate the first peak of the outbreak (2004) and later phase of the outbreak (post-2007).

Importantly, a high relapse fraction reflects a change in the composition of infectious inflow and does

not, by itself, imply an increase in absolute incidence. Consistent with this interpretation, the recovered-to-infectious ratio increases after the primary epidemic peak, making relapse inflow proportionally more influential even as overall case counts decline. Together, these results suggest that relapse becomes increasingly consequential for late-epidemic dynamics and can sustain low-level transmission during the post-peak period. In particular, even when the primary-transmission threshold remains below unity ($R_0 < 1$), relapse can prolong epidemic tails and generate delayed secondary features by continually reseeding infectious compartments without any renewed increase in transmission intensity. This relapse-driven persistence complements the time-series and cumulative-incidence analyses presented earlier. From an epidemiological perspective, these results indicate that uncertainty in relapse-related processes becomes increasingly consequential as the epidemic evolves, even when early transmission dynamics remain similar across scenarios.

6.2 Impact of relapse and time delays under alternative epidemiological scenarios

In this section, we examine how relapse processes and biological time delays shape NiV incidence under a range of alternative epidemiological scenarios. Key parameters are perturbed by $\pm 10\%$ and $\pm 20\%$ around their baseline values, while all remaining parameters are held fixed. The results obtained using joint sensitivity envelopes are summarized in Figure 6. The solid curve denotes the baseline solution, while the shaded region represents the range of epidemic trajectories consistent with the explored scenarios for each parameter pair. These enclosures offer a concise representation of how uncertainty in relapse- and delay-related mechanisms results into variability in epidemic outcomes over time under a variety of epidemiological conditions.

Figures 6(a) and (b) show the joint effects of varying the transmission rate (α) in combination with the relapse rate (ψ_1) and the incubation delay (ω_1), respectively. In both cases, parameter variations influence the magnitude of both the initial outbreak peak and the subsequent epidemic phase, with wider sensitivity envelopes indicating increased model sensitivity under larger perturbations. In contrast, scenarios that combine reduced transmission with a shortened incubation delay consistently suppress incidence across the full simulation period.

Increased treatment of early-stage infectious individuals (τ_1) or increased hospitalization of later-stage infectious individuals (ξ) in conjunction with a reduction in the transmission rate (α) significantly reduces the height of the initial outbreak peak and attenuates the later epidemic hump, as illustrated in Figures 6(c) and (d). These joint effects highlight the importance of combining reductions in transmission with enhanced clinical management.

The later phase of the epidemic is predominantly influenced by the simultaneous reduction of the relapse rate (ψ_1) and enhancement of early-stage treatment (τ_1), as illustrated in Figure 6(e). The initial outbreak peak is only slightly affected, reflecting the fact that relapse-related processes become epidemiologically relevant only after a recovered population has accumulated.

The model exhibits two distinct epidemic phases across all joint parameter combinations. The early outbreak peak is most sensitive to parameters governing primary transmission and progression to infectiousness, such as incubation delay, whereas differences among scenarios become more pronounced during the later phase, when relapse-related mechanisms contribute to sustained transmission. This is reflected in a widening of the sensitivity envelopes after approximately 2007, indicating increasing divergence among epidemic trajectories over time. The individual time-series trajectories underlying the joint sensitivity envelopes show qualitatively similar results (Appendix C, Figure 11).

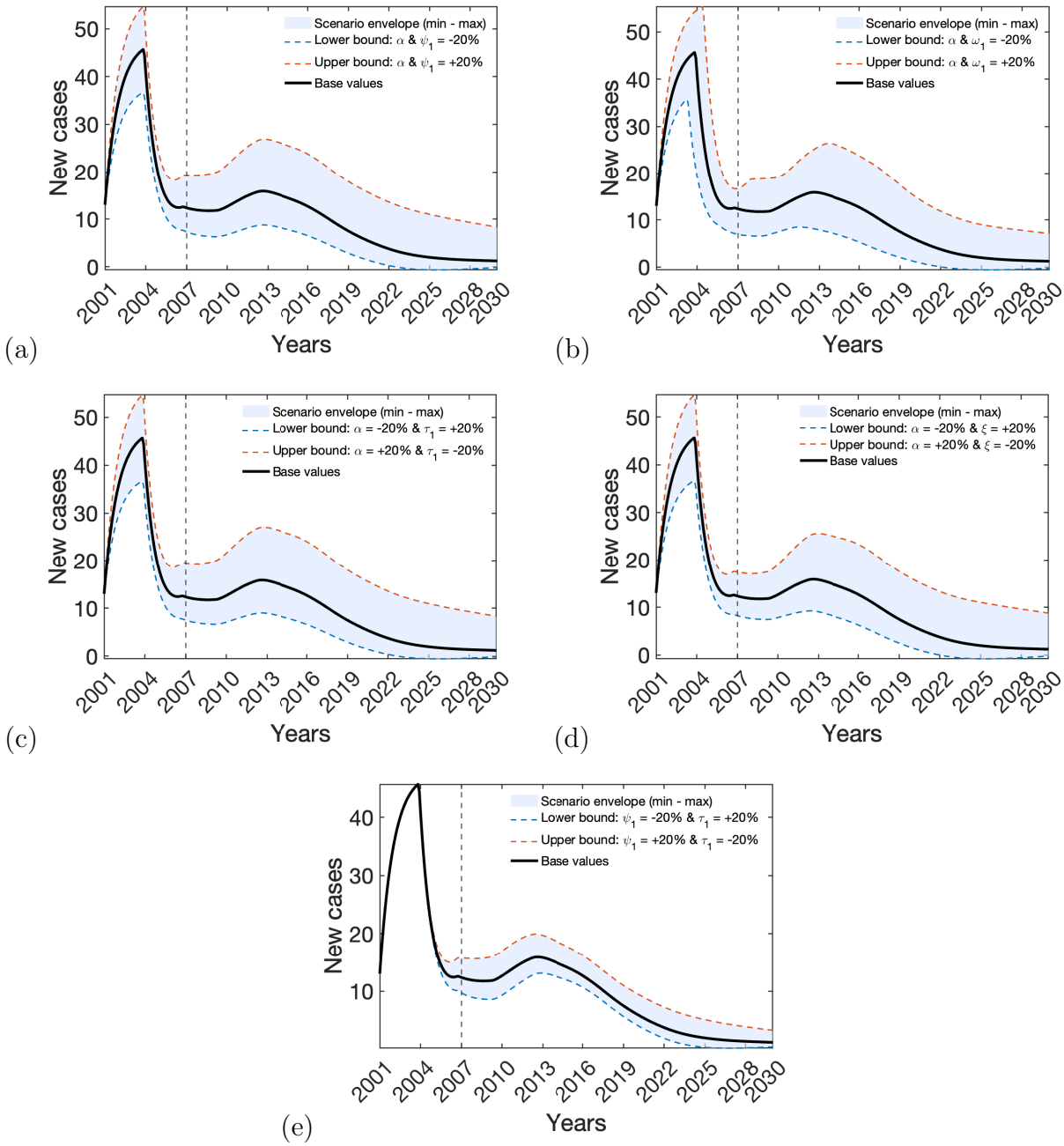

Figure 6: Joint sensitivity envelopes illustrating the combined effects of key epidemiological parameters on NiV incidence. Shaded regions represent the minimum-maximum envelope of incidence trajectories generated by simultaneous perturbations of paired parameters, while the solid black curve denotes the baseline scenario. Panels (a)-(e) correspond to different joint parameter combinations, including concurrent variations in (a) transmission rate (α) and relapse rate (ψ_1), (b) transmission rate (α) and incubation delay (ω_1), (c) transmission rate (α) and treatment rate (τ_1) of early-stage infectious individuals, (d) transmission rate (α) and hospitalization rate (ξ) of later-stage infectious individuals, and (e) relapse rate (ψ_1) and treatment rate (τ_1). Vertical dashed lines indicate the post-2007 period, corresponding to the secondary phase of the outbreak. The widening of the envelopes over time reflects increasing differences among alternative epidemiological scenarios, indicating that long-term epidemic outcomes are more sensitive to parameter variation during the later phase of the epidemic. All parameters are varied simultaneously within a range of $\pm 20\%$ around their baseline values.

6.3 Global sensitivity analysis of R_0

To identify the parameters most strongly influencing the primary-transmission threshold (R_0) , we conducted a global sensitivity analysis using partial rank correlation coefficients (PRCCs), treating R_0 as the response variable. PRCCs measure the strength and direction of each parameter's monotonic influence while accounting for nonlinear interactions among parameters.

The effective human-to-human transmission rate (α) and the recruitment rate (A) have strong positive PRCC values (Figure 7(a)), indicating that increases in either parameter lead to higher values of R_0. Conversely, the natural mortality rate (μ), treatment rate (τ_1), and recovery rate (γ) exhibit strong negative correlations with R_0, reflecting their role in shortening the infectious period and limiting onward transmission. The incubation delay (ω_1) shows a comparatively weak negative influence, indicating that while incubation delay affect epidemic timing, they exert only a limited effect on the invasion threshold itself. Relapse rate (ψ_1) and time delay (ω_2) do not appear explicitly in the expression for R_0 and therefore do not directly influence its value.

We obtain $R_0 \approx 0.047 \ll 1$ for the estimated baseline parameter values, which suggests that sustained transmission driven solely by primary human-to-human contact is highly unlikely. The distribution of R_0 under joint parameter variation is summarized in the box plot in Figure 7(b). It is evident that R_0 remains significantly below unity throughout the explored parameter space. This indicates that the subcritical transmission regime is robust to uncertainty in model parameters.

Importantly, these findings do not contradict the sustained transmission patterns observed in the timeseries simulations. Rather, they highlight a fundamental distinction between invasion potential and long-term persistence. While R_0 governs the ability of primary transmission to initiate an outbreak, it does not capture relapse-mediated mechanisms that operate through the recovered population. As shown in the previous analyses, relapse processes can sustain infection and generate delayed or secondary epidemic features even when R_0 remains far below unity.

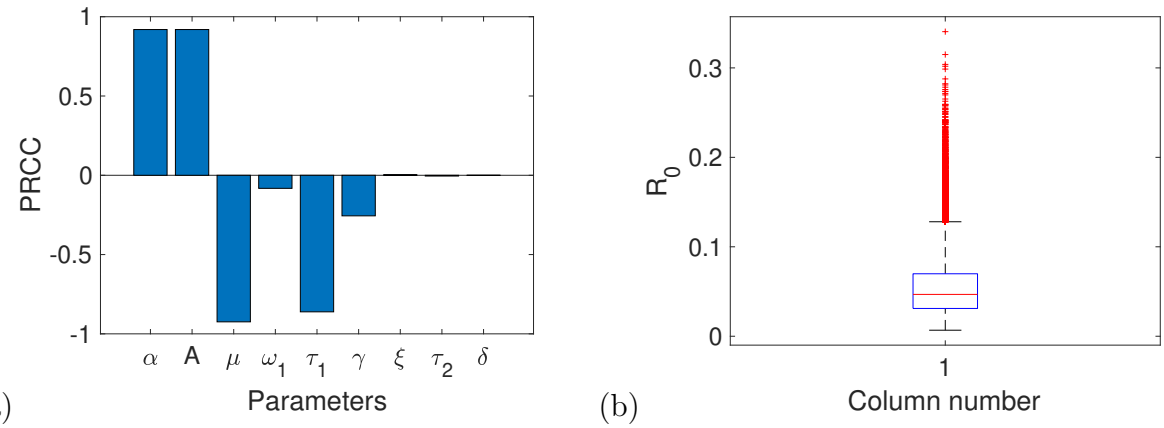

Figure 7: Global sensitivity analysis of the primary-transmission threshold (R_0). (a) Partial rank correlation coefficients (PRCCs) quantifying the monotonic influence of model parameters on the primary-transmission threshold R_0, (b) the corresponding box plot showing the distribution of R_0 under joint parameter variation. Positive (negative) PRCC values indicate parameters that increase (decrease) R_0.

6.4 Numerical simulations of Hopf bifurcation induced by time delays

Under the empirically estimated baseline parameter values, the model does not exhibit Hopf bifurcation within biologically plausible ranges of the delay parameters, indicating that delay-induced oscillatory dynamics are unlikely under current epidemiological conditions. For the estimated parameters, the system exhibits at most damped transient fluctuations, consistent with the observed low-incidence and sporadic nature of reported outbreaks.

To investigate the full dynamical capacity of the proposed model, we consider hypothetical parameter combinations and systematically vary the incubation delay ω_1 and the relapse-associated delay ω_2. Numerical simulations are performed to characterize the asymptotic behavior of the model under alternative delay scenarios. Although sustained oscillations are not supported by current parameter estimates, their emergence under hypothetical conditions highlights the qualitative impact that biological time delays can have on epidemic dynamics and illustrates the broader range of behaviors permitted by the model structure. These simulations reveal transitions from stable equilibria to sustained oscillatory dynamics as the delay parameters exceed critical threshold values, consistent with the occurrence of Hopf bifurcations predicted by the theoretical analysis under the following set of hypothetical parameters: $A = 0.045, \mu = 0.000034, \alpha = 0.4, \tau_1 = 0.25, \tau_2 = 0.75, \gamma = 0.6, \psi_1 = 0.075, \psi_2 = 0.25, \xi = 0.65, \delta = 0.75, \phi_H = 0.09, \phi_T = 0.09, \lambda = 1.0002$ and $\upsilon = 0.1$. Here λ is the progression rate from E to I_1 in the absence of incubation delay.

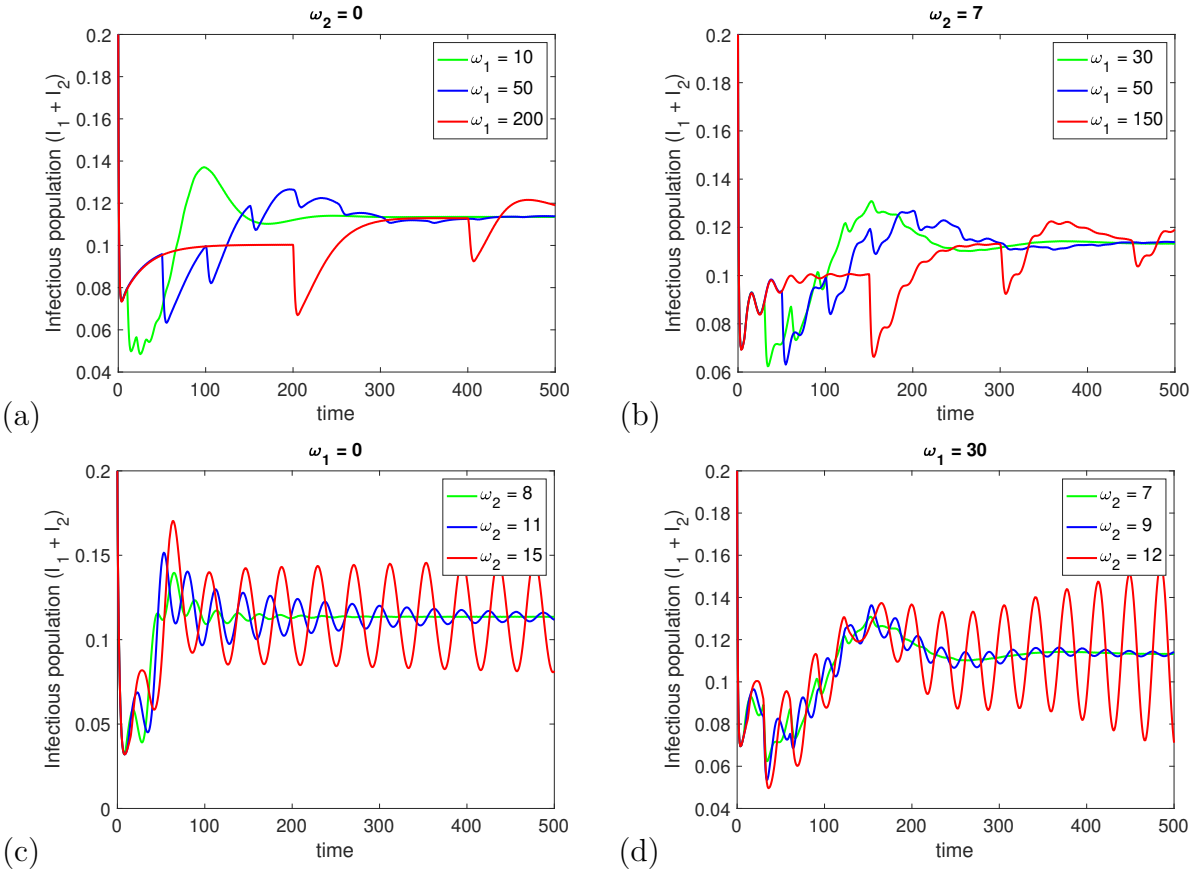

Figure 8: Long-term dynamics of the infectious population $(I_1 + I_2)$ under different combinations of time delays. Panels (a)-(b) show trajectories for varying incubation delay ω_1 with fixed relapse delay $\omega_2 = 0$ and $\omega_2 = 7$, respectively. Panels (c)-(d) show trajectories for varying relapse delay ω_2 with fixed incubation delay $\omega_1 = 0$ and $\omega_1 = 30$, respectively.

We plot the infectious population $(I_1 + I_2)$ for different values of the time-delay parameters ω_1 and ω_2 at the endemic equilibrium. Figure 8 illustrates the dynamics of the total infectious population $(I_1 + I_2)$ under different delay scenarios. When $\omega_2 = 0$ and ω_1 increases (Figure 8(a)), the system transitions from asymptotic stability to sustained periodic oscillations once ω_1 exceeds its critical threshold, indicating a Hopf bifurcation with respect to ω_1. A similar qualitative transition is observed when ω_2 is fixed at a positive value and ω_1 varies (Figure 8(b)), confirming that the incubation delay can act as a bifurcation parameter in multiple delay settings. When $\omega_1 = 0$ (Figure 8(c)), augmenting ω_2 results in a transition from stable convergence to oscillatory behavior beyond a critical threshold. Conversely, when ω_1 is maintained within its stable range (Figure 8(d)), increasing ω_2 similarly induces a shift from asymptotic stability to

persistent oscillations. The numerical simulations align with the previously derived theoretical results for Hopf bifurcation in each instance.

The results indicate that prolonged biological delays can destabilize the endemic equilibrium and produce recurring epidemic cycles. Nevertheless, as these oscillatory regimes emerge solely under hypothetical parameter combinations, they should be interpreted as illustrations of the theoretical dynamical capacity of the model rather than predictions of expected epidemic behavior under current epidemiological conditions.

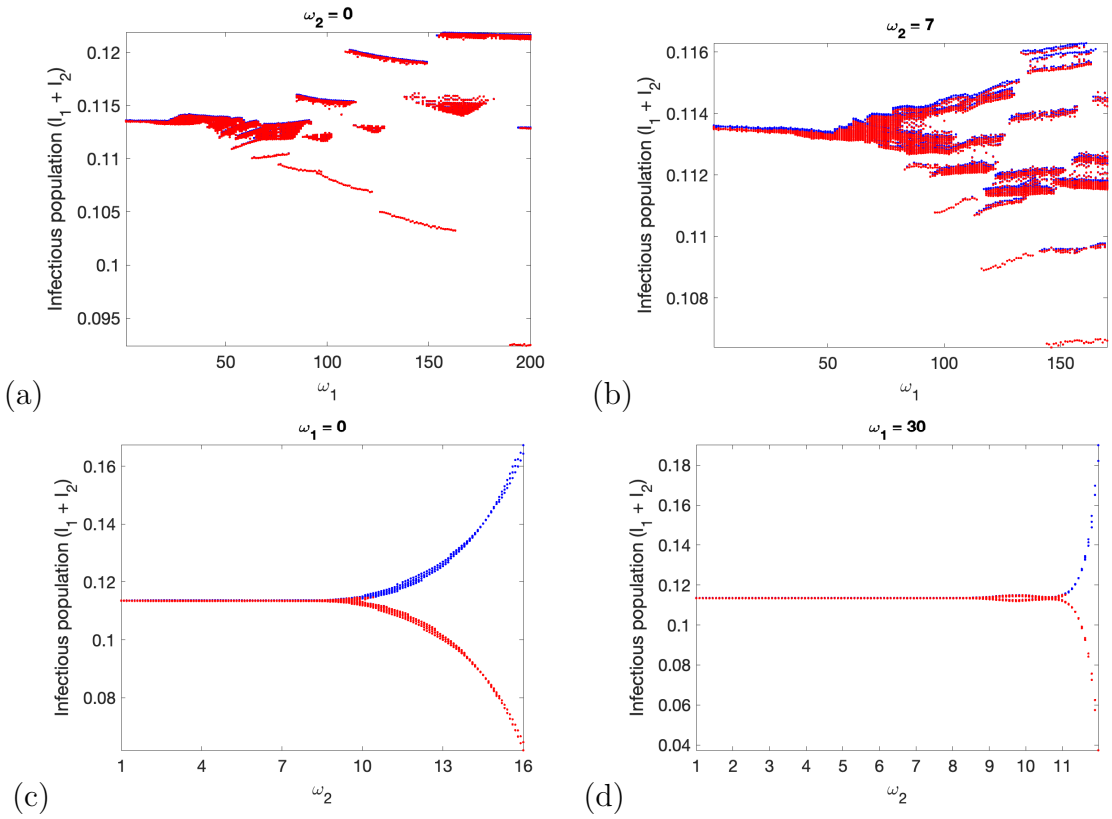

Figure 9: Hopf bifurcation diagrams of the infectious population $(I_1 + I_2)$ in response to alterations in time-delay parameters. Panels (a) and (b) present bifurcation diagrams derived from modifications in the incubation delay ω_1, while maintaining fixed relapse delays of $\omega_2 = 0$ and $\omega_2 = 7$, respectively. Panels (c)-(d) present bifurcation diagrams derived from alterations in the relapse delay ω_2, while maintaining fixed incubation delays of $\omega_1 = 0$ and $\omega_1 = 30$, respectively. The blue and red curves represent the upper and lower limits of the resultant oscillatory solutions.

Furthermore, Figure 9 encapsulates the Hopf bifurcation framework across various delay settings. In Figure 9(a) and (b), augmenting the incubation delay ω_1 past its critical threshold results in a shift from asymptotic stability to sustained periodic oscillations when $\omega_2 = 0$ and when ω_2 is maintained at a positive value, respectively, with ω_1 serving as the bifurcation parameter. In Figure 9(c), surpassing the critical value of the encephalitis delay ω_2 results in the destabilization of the endemic equilibrium, leading to periodic solutions when the incubation delay remains constant. Figure 9(d) further demonstrates that the interaction of both delays alters the amplitude and persistence of oscillations. These results collectively indicate that oscillatory dynamics may emerge from either individual delays or their combined effects, contingent upon the surpassing of relevant critical thresholds.

7 Discussion

Emerging and re-emerging infectious diseases have consistently posed serious threats to both human and animal life. Disease control is frequently hampered not only by initial transmission but also by relapse,

when persons who seem clinically recovered subsequently exhibit symptoms again and may contribute to future transmission. Moreover, intrinsic biological temporal delays, like incubation periods, the delayed onset of severe disease (relapse onset), or delayed therapeutic responses, can further complicate epidemic control by modifying the timing and dynamics of transmission. For NiV disease, a portion of recovered patients subsequently have relapse or delayed-onset encephalitis [18, 20], underscoring the necessity of explicitly considering relapse and temporal delays when evaluating long-term dynamics and formulating control strategies. Numerous mathematical models have analyzed NiV transmission in humans, predominantly concentrating on transmission mechanisms and intervention strategies, including isolation, vaccine, or therapy [25–30]. To date, however, no study has directly examined the synergistic effects of relapse and several biological time delays on NiV dynamics. This study addresses the existing gap by augmenting the model of Tyagi et al. [30] to include relapse and time delays, thereby enabling an analysis of how these mechanisms affect both short- and long-term epidemic dynamics.

Analytical findings for the proposed deterministic delay differential equation (DDE) model indicate that the disease-free equilibrium is locally asymptotically stable if the characteristic roots of the complete linearized delay system reside in the open left half-plane (refer to Section 4). We also establish a clear endemic equilibrium for the comprehensive model with relapse and delineate the corresponding algebraic feasibility requirements. In the absence of relapse, the endemic equilibrium condition simplifies to the traditional persistence criterion $R_0 > 1$. Conversely, in the presence of relapse, the establishment of a positive endemic equilibrium is not solely dictated by the primary-transmission threshold R_0, as relapse feedback alters the effective persistence criterion. Biologically, this indicates that even if direct transmission is inadequate to sustain the disease, relapse may restore the infected population and hinder eradication. The peculiar nature of the endemic equilibrium, assuming it exists, distinguishes this mechanism from traditional backward bifurcation and can be understood as a relapse-driven alteration in the persistence threshold.

Our findings additionally indicate that time delays further influence system stability. When delays are maintained below their critical thresholds, the endemic equilibrium exhibits local asymptotic stability. However, when delays surpass threshold values, stability is compromised by Hopf bifurcation, resulting in persistent oscillations. This mathematically signifies the emergence of periodic solutions; biologically, it relates to recurrent epidemic cycles instead of convergence to a stable endemic state. We further characterized the direction and stability of these oscillations and estimated critical delay lengths using the Nyquist criterion, providing quantitative thresholds at which oscillatory dynamics emerge.

Using reported NiV cases from Bangladesh between 2001 and 2024, we parameterized the model and estimated key epidemiological parameters, including the human-to-human transmission rate (α), disease-induced death rate (δ), relapse rates (ψ_1 and ψ_2), and time delays (ω_1 and ω_2). We further generated forward projections through 2030 to explore potential future trajectories under current epidemiological conditions. A central biological finding is the dominant role of the relapse rate (ψ_1) in governing post-peak epidemic dynamics, even when the primary-transmission threshold remains well below unity. By computing the fraction of relapse contribution to infection dynamics as the proportion of infectious-state replenishment attributable to relapse processes, we show that relapse increasingly drives infection replenishment over time. This explains why low-level transmission can persist even when person-to-person spread is strongly suppressed. Thus, relapse represents a mechanism of persistence that operates independently of classical transmission intensity. Sensitivity and scenario analyses reinforce this conclusion.

Reductions in relapse rate consistently suppress secondary waves and accelerate epidemic fade-out, whereas increase in ψ_1 prolong transmission and increase cumulative incidence. In contrast, reductions in incubation delay (ω_1), interpreted as earlier clinical intervention and faster case detection, primarily reduce and advance the initial epidemic peak and yield the largest reductions in overall case numbers. The time delay associated with encephalitis development (ω_2) has comparatively smaller effects on cumulative incidence but influences the timing and structure of post-recovery transmission. Collectively, these findings indicate that early identification and swift intervention are most efficacious in curbing initial epidemic

proliferation, but relapse-associated mechanisms prevail in long-term sustainability.

From a feasibility standpoint, interventions aimed at reducing the relapse rate (ψ_1) and the effective incubation delay (ω_1) seem more actionable than those influencing the time delay in encephalitis development (ω_2), which is likely dictated by intrinsic biological and clinical mechanisms. Nonetheless, sensitivity to ω_2 offers insight into the temporal dynamics of relapse-driven transmission and may guide post-recovery monitoring measures. Enhanced empirical estimates of relapse timing and frequency would significantly diminish uncertainty in long-term forecasts of epidemic persistence and delayed resurgence, hence improving surveillance strategies.

Joint scenario analyses further illustrated that the effects of relapse rate (ψ_1) and time delays (ω_1 and ω_2) are exacerbated when coupled with fluctuations in transmission and treatment parameters, including reduced transmission intensity (α) or elevated treatment (τ_1) and hospitalization rates (ξ). Concurrent perturbations, such as relapse, delay, and various epidemiological parameters, have more significant impacts than alterations in individual parameters, especially in later years, suggesting a growing divergence in epidemic trajectories over time. This temporal amplification highlights the necessity of continuous long-term surveillance and post-recovery monitoring, as minor variations in relapse-related parameters might result in significantly divergent long-term outcomes.

The estimated basic reproductive number ($R_0 = 0.04$) is much below one, aligning with the sporadic occurrence of reported outbreaks; nevertheless, relapse and delayed disease progression do not directly influence R_0. Thus, methods that exclusively target the reduction of contact-based transmission may prove inadequate for achieving elimination. Long-term management may include rigorous monitoring of recovered patients and improved identification of relapse or delayed-onset disease.

We additionally presented other numerical examples and simulation outcomes to corroborate the analytical results. The model exhibits sensitivity to the length of time delays, with several scenarios demonstrating that stability is compromised when delay parameters surpass their critical thresholds. Numerical simulations, encompassing time-series plots and bifurcation diagrams, consistently corroborate theoretical findings. From a biological standpoint, these results indicate that the incubation period and the onset delay of encephalitis are critical factors influencing epidemic trajectories. Brief delays facilitate disease eradication or stabilization, but extended waits heighten the likelihood of recurrent outbreaks.

Our study possesses multiple limitations. Reliable empirical estimates of relapse frequency remain scarce, and the model presupposes uniform mixing, deterministic dynamics, and constant time delays. The model does not explicitly incorporate spatial structure, stochasticity, behavioral reactions, or distributed delays, all of which may further affect persistence and resurgence. Furthermore, oscillatory dynamics occur solely under hypothetical parameter conditions that exceed existing empirical estimates for NiV, suggesting that these cycles should be viewed as representations of the model's theoretical dynamical potential rather than as forecasts of anticipated epidemic behavior.

Despite these limitations, our results demonstrate that relapse and biological time delays are fundamental components of NiV dynamics and warrant explicit consideration in both modeling studies and surveillance strategies. Similar post-recovery transmission and relapse-associated resurgence have been reported for Ebola and Lassa fever, reinforcing the broader relevance of incorporating relapse-driven mechanisms when modeling emerging zoonotic pathogens. Together, these findings emphasize monitoring recovered individuals and accounting for delayed disease processes are essential for achieving effective disease control.

Conflict of interest

There is no conflict of interest for this research.

Acknowledgments

The research work of Sarita Bugalia and Liliana Salvador was supported by the National Science Foundation (Award # 2200269 "PIPP Phase I: BEHIVE - Behavioral Interaction and Viral Evolution for Pandemic Prevention and Prediction"). The research of Hao Wang was partially supported by the Natural Sciences and Engineering Research Council of Canada (Individual Discovery Grant RGPIN-2025-05734 and Discovery Accelerator Supplement Award PGPAS-2020-00090) and a Canada Research Chair.

References

[1] Rathish B, Vaishnani K (2023) Nipah virus. *StatPearls*, Treasure Island (FL).

[2] Centers for Disease Control and Prevention (2025) Nipah virus (NiV). Available at: `https://stacks.cdc.gov/view/cdc/39019#:~:text=Description%3A,pigs%20in%20Malaysia%20and%20Singapore` (accessed June 2025).

[3] Ahmad SB, Tan CT (2014) Nipah encephalitis-an update. *Medical Journal of Malaysia* **69**:103-111.

[4] Ching PKG, de Los Reyes VC, Sucaldito MN, Tayag E, Columna-Vingno AB, Malbas Jr FF, Bolo Jr GC, Sejvar JJ, Eagles D, Playford G, Dueger E (2015) Outbreak of henipavirus infection, Philippines, 2014. *Emerging Infectious Diseases* **21**:328.

[5] World Health Organization (2026) Nipah virus. Available at: `https://www.who.int/news-room/fact-sheets/detail/nipah-virus` (accessed January 2026).

[6] Jin K, Zhao J, Chen H, Zhang Z, Cao Z, Huang Z, Li H, Liu Y, Ai L, Liu Y, Fan C (2025) On-site visual detection of Nipah virus combining a reverse transcription recombinase-aided amplification with a lateral-flow dipstick assay. *Journal of Integrative Agriculture* **24**:790-794.

[7] Sendow I, Field HE, Adjid A, Ratnawati A, Breed AC, Darminto, Morrissy C, Daniels P (2010) Screening for Nipah virus infection in West Kalimantan province, Indonesia. *Zoonoses and Public Health* **57**:499-503.

[8] Sendow I, Ratnawati A, Taylor T, Adjid RA, Saepulloh M, Barr J, Wong F, Daniels P, Field H (2013) Nipah virus in the fruit bat *Pteropus vampyrus* in Sumatera, Indonesia. *PLoS One* **8**:e69544.

[9] de Araujo J, Lo MK, Tamin A, Ometto TL, Thomazelli LM, Nardi MS, Hurtado RF, Nava A, Spiropoulou CF, Rota PA, Durigon EL (2017) Antibodies against henipa-like viruses in Brazilian bats. *Vector-Borne and Zoonotic Diseases* **17**:271-274.

[10] Drexler JF, Corman VM, Gloza-Rausch F, Seebens A, Annan A, Ipsen A, Kruppa T, Müller MA, Kalko EK, Adu-Sarkodie Y, Oppong S (2009) Henipavirus RNA in African bats. *PLoS One* **4**:e6367.

[11] Field HE, Mackenzie JS, Daszak P (2007) Henipaviruses: emerging paramyxoviruses associated with fruit bats. In: *Wildlife and Emerging Zoonotic Diseases: The Biology, Circumstances and Consequences of Cross-Species Transmission*, 133-159.

[12] Hayman DT, Suu-Ire R, Breed AC, McEachern JA, Wang L, Wood JL, Cunningham AA (2008) Evidence of henipavirus infection in West African fruit bats. *PLoS One* **3**:e2739.

[13] Hsu VP, Hossain MJ, Parashar UD, Ali MM, Ksiazek TG, Kuzmin I, Niezgoda M, Rupprecht C, Bresee J, Breiman RF (2004) Nipah virus encephalitis reemergence, Bangladesh. *Emerging Infectious Diseases* **10**:2082.

[14] Chan YP, Chua KB, Koh CL, Lim ME, Lam SK (2001) Complete nucleotide sequences of Nipah virus isolates from Malaysia. *Journal of General Virology* **82**:2151-2155.

[15] Gurley ES, Montgomery JM, Hossain MJ, Bell M, Azad AK, Islam MR, Molla MAR, Carroll DS, Ksiazek TG, Rota PA, Lowe L (2007) Person-to-person transmission of Nipah virus in a Bangladeshi community. *Emerging Infectious Diseases* **13**:1031.

[16] Luby SP, Hossain MJ, Gurley ES, Ahmed BN, Banu S, Khan SU, Homaira N, Rota PA, Rollin PE, Comer JA, Kenah E (2009) Recurrent zoonotic transmission of Nipah virus into humans, Bangladesh, 2001-2007. *Emerging Infectious Diseases* **15**:1229.

[17] Chattu VK, Kumar R, Kumary S, Kajal F, David JK (2018) Nipah virus epidemic in southern India and emphasizing "One Health" approach to ensure global health security. *Journal of Family Medicine and Primary Care* **7**:275-283.

[18] Goh KJ, Tan CT, Chew NK, Tan PSK, Kamarulzaman A, Sarji SA, Wong KT, Abdullah BJJ, Chua KB, Lam SK (2000) Clinical features of Nipah virus encephalitis among pig farmers in Malaysia. *New England Journal of Medicine* **342**:1229-1235.

[19] Mazzola LT, Kelly-Cirino C (2019) Diagnostics for Nipah virus: a zoonotic pathogen endemic to Southeast Asia. *BMJ Global Health* **4**:e001118.

[20] Tan CT, Goh KJ, Wong KT, Sarji SA, Chua KB, Chew NK, Murugasu P, Loh YL, Chong HT, Tan KS, Thayaparan T (2002) Relapsed and late-onset Nipah encephalitis. *Annals of Neurology* **51**:703-708.

[21] CEPI (2025) Nipah virus. Available at: `https://cepi.net/nipah` (accessed June 2025).

[22] Oxford Vaccine Group (2025) First in-human vaccine trial for Nipah virus. Available at: `https://www.ovg.ox.ac.uk/news/first-in-human-vaccine-trial-for-nipah-virus` (accessed June 2025).

[23] Chong HT, Kamarulzaman A, Tan CT, Goh KJ, Thayaparan T, Kunjapan SR, Chew NK, Chua KB, Lam SK (2001) Treatment of acute Nipah encephalitis with ribavirin. *Annals of Neurology* **49**:810-813.

[24] World Health Organization (2026) Nipah virus infection - India. Available at: `https://www.who.int/emergencies/disease-outbreak-news/item/2023-DON490` (accessed January 2026).

[25] Biswas MHA, Haque MM, Duvvuru G (2015) A mathematical model for understanding the spread of nipah fever epidemic in Bangladesh. In: 2015 International Conference on Industrial Engineering and Operations Management (IEOM), 1-8. IEEE.

[26] Mondal MK, Hanif M, Biswas MHA (2017) A mathematical analysis for controlling the spread of Nipah virus infection. *International Journal of Modelling and Simulation* **37**:185-197.

[27] Khan MY, Ullah S, Farooq M, Al Alwan B, Saqib AB (2024) Optimal control analysis for the Nipah infection with constant and time-varying vaccination and treatment under real data application. *Scientific Reports* **14**:17532.

[28] Xie M, Younas Khan M, Ullah S, Farooq M, Riaz MB, Alwan BA (2025) Optimal control analysis for the transmission of Nipah infection with imperfect vaccination. *PLoS One* **20**:e0317408.

[29] Yu F, Younas Khan M, Bilal Riaz M, Ullah S, Farooq M (2025) Assessing the global dynamics of Nipah infection under vaccination and treatment: a novel computational modeling approach. *PLoS One* **20**:e0309360.

[30] Tyagi S, Martha SC, Abbas S, Debbouche A (2021) Mathematical modeling and analysis for controlling the spread of infectious diseases. *Chaos, Solitons and Fractals* **144**:110707.

[31] Van Den Driessche P, Wang L, Zou X (2007) Modeling diseases with latency and relapse. *Mathematical Biosciences and Engineering* **4**:205-219.

[32] Van den Driessche P, Zou X (2007) Modeling relapse in infectious diseases. *Mathematical Biosciences* **207**:89-103.

[33] Diekmann O, Heesterbeek JA, Roberts MG (2010) The construction of next-generation matrices for compartmental epidemic models. Journal of the royal society interface, 7(47), 873-885.

[34] Van den Driessche P, Watmough J (2002). Reproduction numbers and sub-threshold endemic equilibria for compartmental models of disease transmission. Mathematical biosciences, 180(1-2), 29-48.

[35] Hale JK, Lunel SMV (2013) *Introduction to functional differential equations*, Vol. 99. Springer Science and Business Media.

[36] Hassard BD, Kazarinoff ND, Wan YH (1981) *Theory and applications of Hopf bifurcation*, Vol. 41. CUP Archive.

[37] Benedetto JJ, Czaja W (2009) *Integration and modern analysis*. Boston: Birkhäuser.

[38] Freedman HI, Rao VSH (1983) The trade-off between mutual interference and time lags in predator-prey systems. *Bulletin of Mathematical Biology* **45**:991-1004.

[39] Erbe LH, Freedman HI, Rao VSH (1986) Three-species food-chain models with mutual interference and time delays. *Mathematical Biosciences* **80**:57-80.

[40] IEDCR (2025) Nipah virus transmission in Bangladesh. Available at: `https://iedcr.portal.gov.bd/site/page/d5c87d45-b8cf-4a96-9f94-7170e017c9ce/-` (accessed January 2025).

[41] Worldometers (2024) Bangladesh population. Available at: `https://www.worldometers.info/world-population/bangladesh-population/` (accessed December 2024).

[42] The MathWorks Inc (2024) MATLAB version: 14.6.1 (R2024a). The MathWorks Inc.

[43] Shampine LF, Thompson S (2001) Solving ddes in matlab. *Applied Numerical Mathematics* **37**:441-458.

[44] Lakshmikantham V, Leela S, Martynyuk AA (1989) *Stability analysis of nonlinear systems*. New York: M. Dekker.

Appendix A

Proof of Theorem 2.1: We primarily prove the positivity and boundedness of the solutions of system (2.1) for all $t \geq 0$. For this, we rewrite the first equation of (2.1) at $S = 0$ as

$$\frac{dS}{dt} = A > 0,$$

which pushes $S(t)$ up, implying that positivity of S is preserved.

Further, to prove the positivity of the other variables, we proceed by contradiction using a first time of loss of non-negativity. Assume that there exists a time $t_1 > 0$ such that one of the variables E, I_1, I_2, H, T, R

becomes zero at t_1, while all these variables remain non-negative for all $t \in [0, t_1)$. We discuss the following cases:

$$(1)\ E(t_1) = 0;\ (2)\ I_1(t_1) = 0;\ (3)\ I_2(t_1) = 0;\ (4)\ H(t_1) = 0;\ (5)\ T(t_1) = 0;\ \text{and}\ (6)\ R(t_1) = 0.$$

First, we prove case (2). Let $I_1(t_1) = 0$. Because the initial histories are non-negative on $[-\omega, 0]$ and all state variables remain non-negative on $[0, t_1)$, we have $S(t - \omega_1) \geq 0$, $I_1(t - \omega_1) \geq 0$, $I_2(t - \omega_1) \geq 0$, and $R(t) \geq 0$ for all $t \in [0, t_1)$. Hence

$$\frac{dI_1}{dt} \geq -(\tau_1 + \gamma + \mu)I_1 \quad \text{for all} \quad t \in [0, t_1).$$

By a standard comparison (or Grönwall) argument on $[0, t_1]$, we obtain

$$I_1(t_1) \geq I_1(0)e^{-(\tau_1+\gamma+\mu)t_1} \geq 0,$$

which contradicts the assumption that I_1 becomes negative after t_1. The positivity of the variables I_2, H, and T can be proven in a similar manner.

We further prove case (1): $E(t_1) = 0$. Note that $E(t)$ has an implicit solution given by

$$E(t) = \int_{t-\omega_1}^{t} \alpha S(s)(I_1(s) + I_2(s))e^{-\mu(t-s)}\, ds, \tag{7.1}$$

which represents the accumulated exposed individuals (and follows from the compatibility condition (2.3)). Since $S(t)$, $I_1(t)$, and $I_2(t)$ are non-negative for all relevant times, the integrand is non-negative, and hence $E(t_1) \geq 0$, which contradicts the assumption that E becomes negative after t_1. This implies the positivity of E for $t \geq 0$.

Additionally, we prove case (6): $R(t_1) = 0$. Using the R-equation in (2.1), we obtain

$$\begin{aligned}\frac{dR}{dt}(t_1) &= \phi_H H(t_1) + \phi_T T(t_1) - \mu R(t_1) - \psi_1 R(t_1) - \psi_2 R(t_1 - \omega_2)e^{-\mu\omega_2} \\ &= \phi_H H(t_1) + \phi_T T(t_1) - \psi_2 R(t_1 - \omega_2)e^{-\mu\omega_2}.\end{aligned}$$

By assumption (2.4), it follows that $\frac{dR}{dt}(t_1) \geq 0$. Hence $R(t)$ cannot cross below zero at t_1, which contradicts the assumption that R becomes negative after t_1. Therefore, $R(t) \geq 0$ for all $t \geq 0$.

The total human population is given by

$$N(t) = S(t) + E(t) + I_1(t) + I_2(t) + H(t) + T(t) + R(t). \tag{7.2}$$

Taking derivative of the above equation with respect to time and utilizing (2.1), we have

$$\frac{dN}{dt} = A - \mu N - \delta I_2 - \upsilon\delta H \implies \frac{dN}{dt} \leq A - \mu N.$$

Thus,

$$\limsup_{t\to+\infty} N(t) \leq \frac{A}{\mu}. \tag{7.3}$$

Hence, if $N(t) > \frac{A}{\mu}$, then $\frac{dN}{dt} < 0$. Therefore, by utilizing a standard comparison theorem [44], we have

$$N(t) \leq \frac{A}{\mu} + \left(N(0) - \frac{A}{\mu}\right)e^{-\mu t}, \tag{7.4}$$

where $N(0)$ signifies the initial population size at $t = 0$. Thus, $N(0) \leq \frac{A}{\mu}$ implies $N(t) \leq \frac{A}{\mu}$. If $N(0) > \frac{A}{\mu}$, then the solutions of the system are initially outside of the region Ψ but are ultimately bounded and satisfy $\limsup_{t\to\infty} N(t) \leq A/\mu$. Thus, Ψ is defined by

$$\Psi = \Big\{(S(t), E(t), I_1(t), I_2(t), H(t), T(t), R(t)) \in \mathbb{R}^7_+ : S(t) + E(t) + I_1(t) + I_2(t) + H(t) + T(t) + R(t) \leq \frac{A}{\mu}, \text{ for all } t \geq 0\Big\}. \tag{7.5}$$

Hence, all the solutions of system (2.1) with non-negative initial conditions in Ψ remain in Ψ for $t \geq 0$. Hence, the region Ψ is positively invariant and bounds all the solutions of system (2.1) with non-negative initial conditions. □

Appendix B

Proof of Theorem 4.2: To analyze the local asymptotic stability of D^*, the characteristic equation of the Jacobian of system (2.1) at D^* is computed, which is given by

$$det\begin{pmatrix} P_{11}-\lambda & 0 & P_{13} & P_{14} & 0 & 0 & 0 \\ P_{21}+Q_{21}e^{-\lambda\omega_1} & P_{22}-\lambda & P_{23}+Q_{23}e^{-\lambda\omega_1} & P_{24}+Q_{24}e^{-\lambda\omega_1} & 0 & 0 & 0 \\ Q_{31}e^{-\lambda\omega_1} & 0 & P_{33}+Q_{33}e^{-\lambda\omega_1}-\lambda & Q_{34}e^{-\lambda\omega_1} & 0 & 0 & P_{37} \\ 0 & 0 & P_{43} & P_{44}-\lambda & 0 & 0 & R_{47}e^{-\lambda\omega_2} \\ 0 & 0 & 0 & P_{54} & P_{55}-\lambda & 0 & 0 \\ 0 & 0 & P_{63} & P_{64} & 0 & P_{66}-\lambda & 0 \\ 0 & 0 & 0 & 0 & P_{75} & P_{76} & P_{77}+R_{77}e^{-\lambda\omega_2}-\lambda \end{pmatrix} = 0, \tag{7.6}$$

where

$$\begin{aligned}
&P_{11} = -\mu - \alpha(I_1^* + I_2^*), P_{13} = P_{14} = -\alpha S^*, P_{21} = \alpha(I_1^* + I_2^*), P_{22} = -\mu, P_{23} = P_{24} = \alpha S^*,\\
&P_{33} = -(\tau_1 + \gamma + \mu), P_{37} = \psi_1, P_{43} = \gamma, P_{44} = -(\tau_2 + \xi + \mu + \delta), P_{54} = \xi, P_{55} = -(\phi_H + \mu + \upsilon\delta),\\
&P_{63} = \tau_1, P_{64} = \tau_2, P_{66} = -(\phi_T + \mu), P_{75} = \phi_H, P_{76} = \phi_T, P_{77} = -(\psi_1 + \mu), Q_{21} = -\alpha(I_1^* + I_2^*)e^{-\mu\omega_1},\\
&Q_{23} = Q_{24} = -\alpha S^* e^{-\mu\omega_1}, Q_{31} = \alpha(I_1^* + I_2^*)e^{-\mu\omega_1}, Q_{33} = Q_{34} = \alpha S^* e^{-\mu\omega_1}, R_{47} = \psi_2 e^{-\mu\omega_2}, R_{77} = -\psi_2 e^{-\mu\omega_2}.
\end{aligned}$$

We can write the Eq. (7.6) as

$$\begin{aligned}
&(P_{22}-\lambda)(u_0 + u_1\lambda + u_2\lambda^2 + u_3\lambda^3 + u_4\lambda^4 + u_5\lambda^5 + \lambda^6 + (v_0 + v_1\lambda + v_2\lambda^2 + v_3\lambda^3 + v_4\lambda^4 + v_5\lambda^5)e^{-\lambda\omega_1}\\
&+(w_0 + w_1\lambda + w_2\lambda^2 + w_3\lambda^3 + w_4\lambda^4 + w_5\lambda^5)e^{-\lambda\omega_2} + (x_0 + x_1\lambda + x_2\lambda^2 + x_3\lambda^3 + x_4\lambda^4)e^{-\lambda(\omega_1+\omega_2)}) = 0,
\end{aligned} \tag{7.7}$$

where $u_j, v_j, w_j, j = 0, 1, 2, 3, 4, 5$, and $x_j, j = 0, 1, 2, 3, 4$, are as follows:

$$\begin{aligned}
u_0 =& P_{11}(P_{33}P_{44}P_{55}P_{66}P_{77} - P_{37}(P_{43}(P_{54}P_{66}P_{75} + P_{55}P_{64}P_{76}) - P_{44}P_{55}P_{63}P_{76})),\\
u_1 =& P_{37}(P_{43}(P_{54}P_{66}P_{75} + P_{55}P_{64}P_{76}) - P_{44}P_{55}P_{63}P_{76}) - P_{33}P_{44}P_{55}P_{66}P_{77}\\
&- P_{11}(P_{37}((P_{44} + P_{55})P_{63}P_{76} - P_{43}(P_{54}P_{75} + P_{64}P_{76})) + P_{44}P_{55}P_{66}P_{77}\\
&+ P_{33}(P_{55}P_{66}P_{77} + P_{44}(P_{66}P_{77} + P_{55}(P_{66} + P_{77})))),\\
u_2 =& - P_{37}P_{43}P_{54}P_{75} + P_{37}P_{44}P_{63}P_{76} + P_{37}P_{55}P_{63}P_{76} - P_{37}P_{43}P_{64}P_{76} + P_{44}P_{55}P_{66}P_{77}\\
&+ P_{33}(P_{55}P_{66}P_{77} + P_{44}(P_{66}P_{77} + P_{55}(P_{66} + P_{77})(P_{37}P_{63}P_{76} + P_{55}P_{66}P_{77}\\
&+ P_{44}(P_{66}P_{77} + P_{55}(P_{66} + P_{77})) + P_{33}(P_{66}P_{77} + P_{55}(P_{66} + P_{77}) + P_{44}(P_{55} + P_{66} + P_{77}))),\\
u_3 =& - P_{44}P_{55}P_{66} - P_{44}P_{77}P_{66} - P_{55}P_{77}P_{66} - P_{37}P_{63}P_{76} - P_{44}P_{55}P_{77} - P_{33}(P_{66}P_{77} + P_{55}(P_{66}\\
&+ P_{77}) + P_{44}(P_{55} + P_{66} + P_{77})) - P_{11}(P_{55}P_{66} + P_{77}P_{66} + P_{55}P_{77} + P_{44}(P_{55} + P_{66} + P_{77})\\
&+ P_{33}(P_{44} + P_{55} + P_{66} + P_{77})),
\end{aligned}$$

$$
\begin{aligned}
u_4 =& P_{44}P_{55} + P_{66}P_{55} + P_{44}P_{66} + (P_{44} + P_{55} + P_{66})P_{77} + P_{33}(P_{44} + P_{55} + P_{66} + P_{77}) \\
&+ P_{11}(P_{33} + P_{44} + P_{55} + P_{66} + P_{77}), \quad u_5 = -(P_{11} + P_{33} + P_{44} + P_{55} + P_{66} + P_{77}), \\
v_0 =& P_{55}P_{66}P_{77}(P_{14}P_{43}Q_{31} - P_{13}P_{44}Q_{31} + P_{11}(P_{44}Q_{33} - P_{43}Q_{34})), \\
v_1 =& P_{13}(P_{44}P_{55}P_{66} + (P_{44}P_{55} + (P_{44} + P_{55})P_{66})P_{77})Q_{31} - P_{14}P_{43}(P_{66}P_{77} + P_{55}(P_{66} + P_{77}))Q_{31} \\
&- (P_{11}P_{44}P_{55}P_{66} + (P_{11}P_{44}P_{55} + (P_{11}P_{44} + (P_{11} + P_{44})P_{55})P_{66})P_{77})Q_{33} + P_{43}(P_{11}P_{55}P_{66} \\
&+ (P_{11}P_{55} + (P_{11} + P_{55})P_{66})P_{77})Q_{34}, \\
v_2 =& P_{14}P_{43}(P_{55} + P_{66} + P_{77})Q_{31} - P_{13}(P_{55}P_{66} + (P_{55} + P_{66})P_{77} + P_{44}(P_{55} + P_{66} + P_{77}))Q_{31} \\
&+ (P_{44}P_{55}P_{66} + (P_{55}P_{66} + P_{44}(P_{55} + P_{66}))P_{77} + P_{11}(P_{55}P_{66} + (P_{55} + P_{66})P_{77} + P_{44}(P_{55} \\
&+ P_{66} + P_{77})))Q_{33} - P_{43}(P_{55}P_{66} + (P_{55} + P_{66})P_{77} + P_{11}(P_{55} + P_{66} + P_{77}))Q_{34}, \\
v_3 =& - P_{14}P_{43}Q_{31} + P_{13}(P_{44} + P_{55} + P_{66} + P_{77})Q_{31} - (P_{55}P_{66} + (P_{55} + P_{66})P_{77} + P_{44}(P_{55} \\
&+ P_{66} + P_{77}) + P_{11}(P_{44} + P_{55} + P_{66} + P_{77}))Q_{33} + P_{43}(P_{11} + P_{55} + P_{66} + P_{77})Q_{34}, \\
v_4 =& - P_{13}Q_{31} + (P_{11} + P_{44} + P_{55} + P_{66} + P_{77})Q_{33} - P_{43}Q_{34}, \quad v_5 = -Q_{33}, \\
w_0 =& P_{11}P_{33}(P_{54}P_{66}P_{75}R_{47} + P_{55}(P_{64}P_{76}R_{47} + P_{44}P_{66}R_{77})), \\
w_1 =& P_{11}(-(P_{54}(P_{33} + P_{66})P_{75} + (P_{33} + P_{55})P_{64}P_{76})R_{47} - (P_{44}P_{55}P_{66} + P_{33}(P_{44}P_{55} + (P_{44} \\
&+ P_{55})P_{66}))R_{77}) - P_{33}(P_{54}P_{66}P_{75}R_{47} + P_{55}(P_{64}P_{76}R_{47} + P_{44}P_{66}R_{77})), \\
w_2 =& (P_{54}(P_{33} + P_{66})P_{75} + (P_{33} + P_{55})P_{64}P_{76})R_{47} + (P_{44}P_{55}P_{66} + P_{33}(P_{44}P_{55} + (P_{44} \\
&+ P_{55})P_{66}))R_{77} + P_{11}((P_{54}P_{75} + P_{64}P_{76})R_{47} + (P_{44}P_{55} + (P_{44} + P_{55})P_{66} \\
&+ P_{33}(P_{44} + P_{55} + P_{66}))R_{77}), \\
w_3 =& - (P_{54}P_{75} + P_{64}P_{76})R_{47} - (P_{44}P_{55} + (P_{44} + P_{55})P_{66} + P_{33}(P_{44} + P_{55} + P_{66}) \\
&+ P_{11}(P_{33} + P_{44} + P_{55} + P_{66}))R_{77}, \\
w_4 =& (P_{11} + P_{33} + P_{44} + P_{55} + P_{66})R_{77}, \quad w_5 = -R_{77}, \\
x_0 =& R_{47}(P_{11}P_{54}P_{66}P_{75}Q_{33} + P_{55}P_{76}(P_{14}P_{63}Q_{31} + P_{11}(P_{64}Q_{33} - P_{63}Q_{34}))) \\
&+ P_{55}P_{66}R_{77}(P_{14}P_{43}Q_{31} + P_{11}(P_{44}Q_{33} - P_{43}Q_{34})) - P_{13}Q_{31}(P_{54}P_{66}P_{75}R_{47} \\
&+ P_{55}(P_{64}P_{76}R_{47} + P_{44}P_{66}R_{77})), \\
x_1 =& R_{47}(-(P_{54}(P_{11} + P_{66})P_{75}Q_{33} + P_{76}(P_{14}P_{63}Q_{31} + (P_{11} + P_{55})(P_{64}Q_{33} - P_{63}Q_{34})))) \\
&- R_{77}(P_{14}P_{43}(P_{55} + P_{66})Q_{31} + (P_{11}P_{44}P_{55} + (P_{11}P_{44} + (P_{11} + P_{44})P_{55})P_{66})Q_{33} \\
&- P_{43}(P_{11}P_{55} + (P_{11} + P_{55})P_{66})Q_{34}) + P_{13}Q_{31}((P_{54}P_{75} + P_{64}P_{76})R_{47} + (P_{55}P_{66} \\
&+ P_{44}(P_{55} + P_{66}))R_{77}), \\
x_2 =& R_{47}(P_{54}P_{75}Q_{33} + P_{76}(P_{64}Q_{33} - P_{63}Q_{34})) + R_{77}(P_{14}P_{43}Q_{31} - P_{13}(P_{44} + P_{55} + P_{66})Q_{31} \\
&+ (P_{44}P_{55} + (P_{44} + P_{55})P_{66} + P_{11}(P_{44} + P_{55} + P_{66}))Q_{33} - P_{43}(P_{11} + P_{55} + P_{66})Q_{34}), \\
x_3 =& R_{77}(P_{13}Q_{31} - (P_{11} + P_{44} + P_{55} + P_{66})Q_{33} + P_{43}Q_{34}), \quad x_4 = Q_{33}R_{77}.
\end{aligned}
$$

We first discuss the case when $\omega_1 = \omega_2 = 0$, then the characteristic Eq. (7.7) becomes

$$
i_0 + i_1\lambda + i_2\lambda^2 + i_3\lambda^3 + i_4\lambda^4 + i_5\lambda^5 + \lambda^6 = 0, \tag{7.8}
$$

where

$$
\begin{aligned}
i_0 =& u_0 + v_0 + w_0 + x_0, \quad i_1 = u_1 + v_1 + w_1 + x_1, \\
i_2 =& u_2 + v_2 + w_2 + x_2, \quad i_3 = u_3 + v_3 + w_3 + x_3, \\
i_4 =& u_4 + v_4 + w_4 + x_4, \quad i_5 = u_5 + v_5 + w_5.
\end{aligned}
$$

By utilizing Routh-Hurwitz criterion, we obtain that $Re(\lambda) < 0$ if and only if

$$i_0 > 0, \quad \det\begin{pmatrix} i_5 & 1 \\ i_3 & i_4 \end{pmatrix} > 0, \quad \det\begin{pmatrix} i_5 & 1 & 0 \\ i_3 & i_4 & i_5 \\ i_1 & i_2 & i_3 \end{pmatrix} > 0, \quad \det\begin{pmatrix} i_5 & 1 & 0 & 0 \\ i_3 & i_4 & i_5 & 1 \\ i_1 & i_2 & i_3 & i_4 \\ 0 & i_0 & i_1 & i_2 \end{pmatrix} > 0,$$

$$\det\begin{pmatrix} i_5 & 1 & 0 & 0 & 0 \\ i_3 & i_4 & i_5 & 1 & 0 \\ i_1 & i_2 & i_3 & i_4 & i_5 \\ 0 & i_0 & i_1 & i_2 & i_3 \\ 0 & 0 & 0 & i_0 & i_1 \end{pmatrix} > 0,$$

implying the local asymptotic stability of D^* when $\omega_1 = \omega_2 = 0$. □

Proof of Theorem 4.3: When $\omega_1 > 0$, and $\omega_2 = 0$, then the characteristic Eq. (7.7) becomes

$$\begin{aligned} g_0 + g_1\lambda + g_2\lambda^2 + g_3\lambda^3 + g_4\lambda^4 + g_5\lambda^5 + \lambda^6 \\ + (h_0 + h_1\lambda + h_2\lambda^2 + h_3\lambda^3 + h_4\lambda^4 + h_5\lambda^5)e^{-\lambda\omega_1} = 0, \end{aligned} \tag{7.9}$$

where

$$\begin{aligned} &g_0 = u_0 + w_0, g_1 = u_1 + w_1, g_2 = u_2 + w_2, g_3 = u_3 + w_3, g_4 = u_4 + w_4, g_5 = u_5 + w_5, \\ &h_0 = v_0 + x_0, h_1 = v_1 + x_1, h_2 = v_2 + x_2, h_3 = v_3 + x_3, h_4 = v_4 + x_4, h_5 = v_5. \end{aligned}$$

Let $\lambda = ip_3$ ($p_3 > 0$) be a root of Eq. (7.9). We have

$$a_4\cos(p_3\omega_1) + b_4\sin(p_3\omega_1) = c_4, \quad b_4\cos(p_3\omega_1) - a_4\sin(p_3\omega_1) = d_4, \tag{7.10}$$

where

$$\begin{aligned} &a_4 = h_4p_3^4 - h_2p_3^2 + h_0, \quad b_4 = h_5p_3^5 - h_3p_3^3 + h_1p_3, \\ &c_4 = -g_4p_3^4 + g_2p_3^2 - g_0 + p_3^6, \quad d_4 = -g_5p_3^5 + g_3p_3^3 - g_1p_3^5. \end{aligned}$$

From Eq. (7.10), we have

$$a_4^2 + b_4^2 = c_4^2 + d_4^2 \implies p_3^{12} + n_{11}p_3^{10} + n_{12}p_3^8 + n_{13}p_3^6 + n_{14}p_3^4 + n_{15}p_3^2 + n_{16} = 0, \tag{7.11}$$

where

$$\begin{aligned} n_{11} =& g_5^2 - 2g_4 - h_5^2, \quad n_{12} = g_4^2 + 2g_2 - 2g_3g_5 - h_4^2 + 2h_3h_5, \\ n_{13} =& g_3^2 - 2g_0 - 2g_2g_4 + 2g_1g_5 - h_3^2 + 2h_2h_4 - 2h_1h_5, \\ n_{14} =& g_2^2 - 2g_1g_3 + 2g_0g_4 - h_2^2 + 2h_1h_3 - 2h_0h_4, \\ n_{15} =& g_1^2 - 2g_0g_2 - h_1^2 + 2h_0h_2, \quad n_{16} = g_0^2 - h_0^2. \end{aligned}$$

Let $p_3^2 = q_3$, then Eq. (7.11) becomes in the following form:

$$q_3^6 + n_{11}q_3^5 + n_{12}q_3^4 + n_{13}q_3^3 + n_{14}q_3^2 + n_{15}q_3 + n_{16} = 0. \tag{7.12}$$

Assume that **H1:** Eq. (7.12) has a positive root q_{30}, then Eq. (7.11) also has a positive root $p_{30} = \sqrt{q_{30}}$. Furthermore, eradicating $\sin(p_3\omega_1)$ from Eq. (7.10) and replacing p_3 with p_{30}, we obtain

$$\omega_1' = \frac{1}{p_{30}} \times \left\{\arccos\left(\frac{a_4c_4 + b_4d_4}{a_4^2 + b_4^2}\right)\right\}. \tag{7.13}$$

Now, differentiating Eq. (7.9) with respect to ω_1, using $\lambda = ip_{30}$ and simplifying, we obtain

$$Re\left(\frac{d\lambda}{d\omega_1}\right)^{-1}_{\lambda=ip_{30}} = \frac{\tilde{M}_{41}\tilde{M}_{42} + \tilde{M}_{43}\tilde{M}_{44}}{\tilde{M}_{42}^2 + \tilde{M}_{44}^2}, \tag{7.14}$$

where

$$\begin{aligned}
\tilde{M}_{41} =& h_4 p_{30}^5 \sin(p_{30}\omega_1) - h_2 p_{30}^3 \sin(p_{30}\omega_1) + h_0 p_{30} \sin(p_{30}\omega_1) + h_5 p_{30}^6(-\cos(p_{30}\omega_1)) \\
&+ h_3 p_{30}^4 \cos(p_{30}\omega_1) - h_1 p_{30}^2 \cos(p_{30}\omega_1), \\
\tilde{M}_{42} =& p_{30}^4(5g_5 + 5h_5\cos(p_{30}\omega_1) - h_4\omega_1\cos(p_{30}\omega_1)) + p_{30}^2(-3g_3 - 3h_3\cos(p_{30}\omega_1) \\
&+ h_2\omega_1\cos(p_{30}\omega_1)) + g_1 + h_5 p_{30}^5\omega_1(-\sin(p_{30}\omega_1)) + p_{30}^3(h_3\omega_1\sin(p_{30}\omega_1) \\
&- 4h_4\sin(p_{30}\omega_1)) + p_{30}(2h_2\sin(p_{30}\omega_1) - h_1\omega_1\sin(p_{30}\omega_1)) + h_1\cos(p_{30}\omega_1) \\
&- h_0\omega_1\cos(p_{30}\omega_1), \\
\tilde{M}_{43} =& h_5 p_{30}^6 \sin(p_{30}\omega_1) - h_3 p_{30}^4 \sin(p_{30}\omega_1) + h_1 p_{30}^2 \sin(p_{30}\omega_1) + h_4 p_{30}^5 \cos(p_{30}\omega_1) \\
&- h_2 p_{30}^3 \cos(p_{30}\omega_1) + h_0 p_{30} \cos(p_{30}\omega_1), \\
\tilde{M}_{44} =& p_{30}^3(-4g_4 - 4h_4\cos(p_{30}\omega_1) + h_3\omega_1\cos(p_{30}\omega_1)) + p_{30}(2g_2 + 2h_2\cos(p_{30}\omega_1) \\
&- h_1\omega_1\cos(p_{30}\omega_1)) + p_{30}^4(h_4\omega_1\sin(p_{30}\omega_1) - 5h_5\sin(p_{30}\omega_1)) + p_{30}^2(3h_3\sin(p_{30}\omega_1) \\
&- h_2\omega_1\sin(p_{30}\omega_1)) - h_1\sin(p_{30}\omega_1) + h_0\omega_1\sin(p_{30}\omega_1) + p_{30}^5(6 - h_5\omega_1\cos(p_{30}\omega_1)).
\end{aligned}$$

Hence, $Re\left(\frac{d\lambda}{d\omega_1}\right)^{-1}_{\lambda=ip_{30}} \neq 0$ if the condition **H2:** $\tilde{M}_{41}\tilde{M}_{42} + \tilde{M}_{43}\tilde{M}_{44} \neq 0$ holds. Consequently, the Hopf bifurcation theorem [36] implies the Hopf bifurcation in system (2.1). □

Proof of Theorem 4.4: When $\omega_1 = 0$, and $\omega_2 > 0$, then the characteristic Eq. (7.7) becomes

$$\begin{aligned}
k_0 + k_1\lambda + k_2\lambda^2 + k_3\lambda^3 + k_4\lambda^4 + k_5\lambda^5 + \lambda^6 \\
+ (l_0 + l_1\lambda + l_2\lambda^2 + l_3\lambda^3 + l_4\lambda^4 + l_5\lambda^5)e^{-\lambda\omega_2} = 0,
\end{aligned} \tag{7.15}$$

where

$$\begin{aligned}
&k_0 = u_0 + v_0, k_1 = u_1 + v_1, k_2 = u_2 + v_2, k_3 = u_3 + v_3, k_4 = u_4 + v_4, k_5 = u_5 + v_5, \\
&l_0 = w_0 + x_0, l_1 = w_1 + x_1, l_2 = w_2 + x_2, l_3 = w_3 + x_3, l_4 = w_4 + x_4, l_5 = w_5.
\end{aligned}$$

Let $\lambda = ip_4$ ($p_4 > 0$) be a root of Eq. (7.15). We have

$$a_5\cos(p_4\omega_2) + b_5\sin(p_4\omega_2) = c_5, \quad b_5\cos(p_4\omega_2) - a_5\sin(p_4\omega_2) = d_5, \tag{7.16}$$

where

$$\begin{aligned}
a_5 =& l_4 p_4^4 - l_2 p_4^2 + l_0, \quad b_5 = l_5 p_4^5 - l_3 p_4^3 + l_1 p_4, \\
c_5 =& -k_4 p_4^4 + k_2 p_4^2 - k_0 + p_4^6, \quad d_5 = -k_5 p_4^5 + k_3 p_4^3 - k_1 p_4^5.
\end{aligned}$$

From Eq. (7.16), we obtain

$$a_5^2 + b_5^2 = c_5^2 + d_5^2 \implies p_4^{12} + \tilde{n}_{11}p_4^{10} + \tilde{n}_{12}p_4^8 + \tilde{n}_{13}p_4^6 + \tilde{n}_{14}p_4^4 + \tilde{n}_{15}p_4^2 + \tilde{n}_{16} = 0, \tag{7.17}$$

where

$$\begin{aligned}
\tilde{n}_{11} =& k_5^2 - 2k_4 - l_5^2, \quad \tilde{n}_{12} = k_4^2 + 2k_2 - 2k_3k_5 - l_4^2 + 2l_3l_5, \\
\tilde{n}_{13} =& k_3^2 - 2k_0 - 2k_2k_4 + 2k_1k_5 - l_3^2 + 2l_2l_4 - 2l_1l_5, \\
\tilde{n}_{14} =& k_2^2 - 2k_1k_3 + 2k_0k_4 - l_2^2 + 2l_1l_3 - 2l_0l_4, \\
\tilde{n}_{15} =& k_1^2 - 2k_0k_2 - l_1^2 + 2l_0l_2, \quad \tilde{n}_{16} = k_0^2 - l_0^2.
\end{aligned}$$

Let $p_4^2 = q_4$. Eq. (7.17) becomes in the following form:

$$q_4^6 + \tilde{n}_{11}q_4^5 + \tilde{n}_{12}q_4^4 + \tilde{n}_{13}q_4^3 + \tilde{n}_{14}q_4^2 + \tilde{n}_{15}q_4 + \tilde{n}_{16} = 0. \tag{7.18}$$

Assume that **H3:** Eq. (7.18) has a positive root q_{40}, then Eq. (7.17) also has a positive root $p_{40} = \sqrt{q_{40}}$. Furthermore, eradicating $\sin(p_4\omega_2)$ from Eq. (7.16) and replacing p_4 with p_{40}, we obtain

$$\omega_2' = \frac{1}{p_{40}} \times \left\{ \arccos\left(\frac{a_5c_5 + b_5d_5}{a_5^2 + b_5^2} \right) \right\}. \tag{7.19}$$

Now, differentiating Eq. (7.15) with respect to ω_2, replacing $\lambda = ip_{40}$ and simplifying we obtain

$$Re\left(\frac{d\lambda}{d\omega_2}\right)^{-1}_{\lambda=ip_{40}} = \frac{\tilde{M}_{51}\tilde{M}_{52} + \tilde{M}_{53}\tilde{M}_{54}}{\tilde{M}_{52}^2 + \tilde{M}_{54}^2}, \tag{7.20}$$

where

$$\begin{aligned}
\tilde{M}_{51} =& l_4p_{40}^5\sin(p_{40}\omega_2) - l_2p_{40}^3\sin(p_{40}\omega_2) + l_0p_{40}\sin(p_{40}\omega_2) + l_5p_{40}^6(-\cos(p_{40}\omega_2)) \\
&+ l_3p_{40}^4\cos(p_{40}\omega_2) - l_1p_{40}^2\cos(p_{40}\omega_2), \\
\tilde{M}_{52} =& p_{40}^4(5k_5 + 5l_5\cos(p_{40}\omega_2) - l_4\omega_2\cos(p_{40}\omega_2)) + p_{40}^2(-3k_3 - 3l_3\cos(p_{40}\omega_2) \\
&+ l_2\omega_2\cos(p_{40}\omega_2)) + k_1 + l_5p_{40}^5\omega_2(-\sin(p_{40}\omega_2)) + p_{40}^3(l_3\omega_2\sin(p_{40}\omega_2) \\
&- 4l_4\sin(p_{40}\omega_2)) + p_{40}(2l_2\sin(p_{40}\omega_2) - l_1\omega_2\sin(p_{40}\omega_2)) + l_1\cos(p_{40}\omega_2) \\
&- l_0\omega_2\cos(p_{40}\omega_2), \\
\tilde{M}_{53} =& l_5p_{40}^6\sin(p_{40}\omega_2) - l_3p_{40}^4\sin(p_{40}\omega_2) + l_1p_{40}^2\sin(p_{40}\omega_2) + l_4p_{40}^5\cos(p_{40}\omega_2) \\
&- l_2p_{40}^3\cos(p_{40}\omega_2) + l_0p_{40}\cos(p_{40}\omega_2), \\
\tilde{M}_{54} =& p_{40}^3(-4k_4 - 4l_4\cos(p_{40}\omega_2) + l_3\omega_2\cos(p_{40}\omega_2)) + p_{40}(2k_2 + 2l_2\cos(p_{40}\omega_2) \\
&- l_1\omega_2\cos(p_{40}\omega_2)) + p_{40}^4(l_4\omega_2\sin(p_{40}\omega_2) - 5l_5\sin(p_{40}\omega_2)) + p_{40}^2(3l_3\sin(p_{40}\omega_2) \\
&- l_2\omega_2\sin(p_{40}\omega_2)) - l_1\sin(p_{40}\omega_2) + l_0\omega_2\sin(p_{40}\omega_2) + p_{40}^5(6 - l_5\omega_2\cos(p_{40}\omega_2)).
\end{aligned}$$

Hence, $Re\left(\frac{d\lambda}{d\omega_2}\right)^{-1}_{\lambda=ip_{40}} \neq 0$ if the condition **H4:** $\tilde{M}_{51}\tilde{M}_{52} + \tilde{M}_{53}\tilde{M}_{54} \neq 0$ holds. Consequently, the Hopf bifurcation theorem [36] implies the Hopf bifurcation in system (2.1). □

Proof of Theorem 4.5: When $\omega_1 > 0$ and $\omega_2 \in [0, \omega_2')$. In this case, we take ω_1 as bifurcation parameter and ω_2 in stable interval. We can write Eq. (7.7) in the following form:

$$\begin{aligned}
&u_0 + u_1\lambda + u_2\lambda^2 + u_3\lambda^3 + u_4\lambda^4 + u_5\lambda^5 + \lambda^6 + (w_0 + w_1\lambda + w_2\lambda^2 + w_3\lambda^3 + w_4\lambda^4 + w_5\lambda^5)e^{-\lambda\omega_2} \\
&+ (v_0 + v_1\lambda + v_2\lambda^2 + v_3\lambda^3 + v_4\lambda^4 + v_5\lambda^5 + (x_0 + x_1\lambda + x_2\lambda^2 + x_3\lambda^3 + x_4\lambda^4)e^{-\lambda\omega_2})e^{-\lambda\omega_1} = 0.
\end{aligned} \tag{7.21}$$

Let $\lambda = ip_5$ ($p_5 > 0$) be a root of Eq. (7.21). We have

$$a_6\cos(p_5\omega_1) + b_6\sin(p_5\omega_1) = c_6, \quad b_6\cos(p_5\omega_1) - a_6\sin(p_5\omega_1) = d_6, \tag{7.22}$$

where

$$\begin{aligned}
a_6 =& p_5^4v_4 - p_5^2v_2 + v_0 + \left(p_5x_1 - p_5^3x_3\right)\sin\left(p_5\omega_2\right) + \left(p_5^4x_4 - p_5^2x_2 + x_0\right)\cos\left(p_5\omega_2\right), \\
b_6 =& p_5^5v_5 - p_5^3v_3 + p_5v_1 - \left(p_5^4x_4 - p_5^2x_2 + x_0\right)\sin\left(p_5\omega_2\right) + \left(p_5x_1 - p_5^3x_3\right)\cos\left(p_5\omega_2\right), \\
c_6 =& -\left(p_5^4u_4 - p_5^2u_2 - p_5^6 + u_0\right) - \left(p_5^5w_5 - p_5^3w_3 + p_5w_1\right)\sin\left(p_5\omega_2\right) + \left(p_5^4w_4 - p_5^2w_2 + w_0\right)\left(-\cos\left(p_5\omega_2\right)\right), \\
d_6 =& -\left(p_5^5u_5 - p_5^3u_3 + p_5u_1\right) + \left(p_5^4w_4 - p_5^2w_2 + w_0\right)\sin\left(p_5\omega_2\right) - \left(p_5^5w_5 - p_5^3w_3 + p_5w_1\right)\cos\left(p_5\omega_2\right).
\end{aligned}$$

From Eq. (7.22), we have

$$a_6^2 + b_6^2 = c_6^2 + d_6^2. \tag{7.23}$$

Assume that **H5:** Eq. (7.23) has a positive root p_{50}. Furthermore, eradicating $\sin(p_5\omega_1)$ from Eq. (7.22) and replacing p_5 by p_{50}, we obtain

$$\omega'_{11} = \frac{1}{p_{50}} \times \left\{ \arccos\left(\frac{a_6c_6 + b_6d_6}{a_6^2 + b_6^2} \right) \right\}. \tag{7.24}$$

Further, differentiating Eq. (7.21) with respect to ω_1, putting $\lambda = ip_{50}$ and simplifying, we obtain

$$Re\left(\frac{d\lambda}{d\omega_1}\right)^{-1}_{\lambda=ip_{50}} = \frac{\tilde{M}_{61}\tilde{M}_{62} + \tilde{M}_{63}\tilde{M}_{64}}{\tilde{M}_{62}^2 + \tilde{M}_{64}^2}, \tag{7.25}$$

where

$$\begin{aligned}
\tilde{M}_{61} =& p_{50}^5(v_4(-\sin(p_{50}\omega_1)) - x_4\sin(p_{50}\omega_1)\cos(p_{50}\omega_2) + x_4\sin(p_{50}\omega_2)\cos(p_{50}\omega_1)) \\
&+ p_{50}^4(v_3\cos(p_{50}\omega_1) + x_3\sin(p_{50}\omega_1)\sin(p_{50}\omega_2) + x_3\cos(p_{50}\omega_1)\cos(p_{50}\omega_2)) \\
&+ p_{50}^3(v_2\sin(p_{50}\omega_1) + x_2\sin(p_{50}\omega_1)\cos(p_{50}\omega_2) - x_2\sin(p_{50}\omega_2)\cos(p_{50}\omega_1)) \\
&+ p_{50}^2(v_1(-\cos(p_{50}\omega_1)) - x_1\sin(p_{50}\omega_1)\sin(p_{50}\omega_2) - x_1\cos(p_{50}\omega_1)\cos(p_{50}\omega_2)) \\
&+ p_{50}(v_0(-\sin(p_{50}\omega_1)) - x_0\sin(p_{50}\omega_1)\cos(p_{50}\omega_2) + x_0\sin(p_{50}\omega_2)\cos(p_{50}\omega_1)) \\
&+ p_{50}^6(-\cos(p_{50}\omega_1)),
\end{aligned}$$

$$\begin{aligned}
\tilde{M}_{62} =& (-\sin(p_{50}\omega_1)\omega_1 - \sin(p_{50}\omega_2)w_5\omega_2)p_{50}^5 + (v_4\omega_1\cos(p_{50}\omega_1) \\
&+ \cos(p_{50}\omega_2)x_4\omega_1\cos(p_{50}\omega_1) + 5\cos(p_{50}\omega_1) + 5u_5 + 5\cos(p_{50}\omega_2)w_5 \\
&+ \sin(p_{50}\omega_1)\sin(p_{50}\omega_2)x_4\omega_1 - \cos(p_{50}\omega_2)w_4\omega_2 - \cos(p_{50}(\omega_1-\omega_2))x_4\omega_2)p_{50}^4 \\
&+ (4\sin(p_{50}\omega_1)v_4 - 4\sin(p_{50}\omega_2)w_4 + 4\sin(p_{50}(\omega_1-\omega_2))x_4 + \sin(p_{50}\omega_1)v_3\omega_1 \\
&+ \cos(p_{50}\omega_2)\sin(p_{50}\omega_1)x_3\omega_1 - \cos(p_{50}\omega_1)\sin(p_{50}\omega_2)x_3\omega_1 + \sin(p_{50}\omega_2)w_3\omega_2 \\
&- \sin(p_{50}(\omega_1-\omega_2))x_3\omega_2)p_{50}^3 + (-3u_3 - 3\cos(p_{50}\omega_1)v_3 - 3\cos(p_{50}\omega_2)w_3 \\
&- 3\cos(p_{50}(\omega_1-\omega_2))x_3 - \cos(p_{50}\omega_1)v_2\omega_1 - \cos(p_{50}\omega_1)\cos(p_{50}\omega_2)x_2\omega_1 \\
&- \sin(p_{50}\omega_1)\sin(p_{50}\omega_2)x_2\omega_1 + \cos(p_{50}\omega_2)w_2\omega_2 + \cos(p_{50}(\omega_1-\omega_2))x_2\omega_2)p_{50}^2 \\
&+ (-2\sin(p_{50}\omega_1)v_2 + 2\sin(p_{50}\omega_2)w_2 - 2\sin(p_{50}(\omega_1-\omega_2))x_2 - \sin(p_{50}\omega_1)v_1\omega_1 \\
&- \cos(p_{50}\omega_2)\sin(p_{50}\omega_1)x_1\omega_1 + \cos(p_{50}\omega_1)\sin(p_{50}\omega_2)x_1\omega_1 - \sin(p_{50}\omega_2)w_1\omega_2 \\
&+ \sin(p_{50}(\omega_1-\omega_2))x_1\omega_2)p_{50} + u_1 + \cos(p_{50}\omega_1)v_1 + \cos(p_{50}\omega_2)w_1 \\
&+ \cos(p_{50}(\omega_1-\omega_2))x_1 + \cos(p_{50}\omega_1)v_0\omega_1 + \cos(p_{50}\omega_1)\cos(p_{50}\omega_2)x_0\omega_1 \\
&+ \sin(p_{50}\omega_1)\sin(p_{50}\omega_2)x_0\omega_1 - \cos(p_{50}\omega_2)w_0\omega_2 - \cos(p_{50}(\omega_1-\omega_2))x_0\omega_2,
\end{aligned}$$

$$\begin{aligned}
\tilde{M}_{63} =& p_{50}^4(-x_3\log(e)\sin(p_{50}\omega_2)\cos(p_{50}\omega_1) + v_3\sin(p_{50}\omega_1) + x_3\sin(p_{50}\omega_1)\cos(p_{50}\omega_2)) \\
&+ p_{50}^5(v_4\cos(p_{50}\omega_1) + x_4\sin(p_{50}\omega_1)\sin(p_{50}\omega_2) + x_4\cos(p_{50}\omega_1)\cos(p_{50}\omega_2)) \\
&+ p_{50}^3(v_2(-\cos(p_{50}\omega_1)) - x_2\sin(p_{50}\omega_1)\sin(p_{50}\omega_2) - x_2\cos(p_{50}\omega_1)\cos(p_{50}\omega_2)) \\
&+ p_{50}^2(v_1(-\sin(p_{50}\omega_1)) - x_1\sin(p_{50}\omega_1)\cos(p_{50}\omega_2) + x_1\sin(p_{50}\omega_2)\cos(p_{50}\omega_1)) \\
&+ p_{50}(v_0\cos(p_{50}\omega_1) + x_0\sin(p_{50}\omega_1)\sin(p_{50}\omega_2) + x_0\cos(p_{50}\omega_1)\cos(p_{50}\omega_2)) \\
&+ p_{50}^6(-\sin(p_{50}\omega_1)),
\end{aligned}$$

$$
\begin{aligned}
\tilde{M}_{64} =&(\cos(p_{50}\omega_1)\omega_1 - \cos(p_{50}\omega_2)w_5\omega_2 + 6)p_{50}^5 + (v_4\omega_1 \sin(p_{50}\omega_1) \\
&+ \cos(p_{50}\omega_2)x_4\omega_1 \sin(p_{50}\omega_1) + 5\sin(p_{50}\omega_1) - 5\sin(p_{50}\omega_2)w_5 \\
&- \cos(p_{50}\omega_1)\sin(p_{50}\omega_2)x_4\omega_1 + \sin(p_{50}\omega_2)w_4\omega_2 - \sin(p_{50}(\omega_1-\omega_2))x_4\omega_2)p_{50}^4 \\
&+ (-4u_4 - 4\cos(p_{50}\omega_1)v_4 - 4\cos(p_{50}\omega_2)w_4 - 4\cos(p_{50}(\omega_1-\omega_2))x_4 \\
&- \cos(p_{50}\omega_1)v_3\omega_1 - \cos(p_{50}\omega_1)\cos(p_{50}\omega_2)x_3\omega_1 - \sin(p_{50}\omega_1)\sin(p_{50}\omega_2)x_3\omega_1 \\
&+ \cos(p_{50}\omega_2)w_3\omega_2 + \cos(p_{50}(\omega_1-\omega_2))x_3\omega_2)p_{50}^3 + (-3\sin(p_{50}\omega_1)v_3 + 3\sin(p_{50}\omega_2)w_3 \\
&- 3\sin(p_{50}(\omega_1-\omega_2))x_3 - \sin(p_{50}\omega_1)v_2\omega_1 - \cos(p_{50}\omega_2)\sin(p_{50}\omega_1)x_2\omega_1 \\
&+ \cos(p_{50}\omega_1)\sin(p_{50}\omega_2)x_2\omega_1 - \sin(p_{50}\omega_2)w_2\omega_2 + \sin(p_{50}(\omega_1-\omega_2))x_2\omega_2)p_{50}^2 \\
&+ (2u_2 + 2\cos(p_{50}\omega_1)v_2 + 2\cos(p_{50}\omega_2)w_2 + 2\cos(p_{50}(\omega_1-\omega_2))x_2 + \cos(p_{50}\omega_1)v_1\omega_1 \\
&+ \cos(p_{50}\omega_1)\cos(p_{50}\omega_2)x_1\omega_1 + \sin(p_{50}\omega_1)\sin(p_{50}\omega_2)x_1\omega_1 - \cos(p_{50}\omega_2)w_1\omega_2 \\
&- \cos(p_{50}(\omega_1-\omega_2))x_1\omega_2)p_{50} + \sin(p_{50}\omega_1)v_1 - \sin(p_{50}\omega_2)w_1 + \sin(p_{50}(\omega_1-\omega_2))x_1 \\
&+ \sin(p_{50}\omega_1)v_0\omega_1 + \cos(p_{50}\omega_2)\sin(p_{50}\omega_1)x_0\omega_1 - \cos(p_{50}\omega_1)\sin(p_{50}\omega_2)x_0\omega_1 \\
&+ \sin(p_{50}\omega_2)w_0\omega_2 - \sin(p_{50}(\omega_1-\omega_2))x_0\omega_2.
\end{aligned}
$$

Hence, $Re\left(\frac{d\lambda}{d\omega_1}\right)^{-1}_{\lambda=ip_{50}} \neq 0$ if the condition **H6:** $\tilde{M}_{61}\tilde{M}_{62} + \tilde{M}_{63}\tilde{M}_{64} \neq 0$ holds. Consequently, the Hopf bifurcation theorem [36] implies the Hopf bifurcation in system (2.1). □

Properties of Hopf bifurcation: Here, we present the detailed derivation of the corresponding linear operator formulation, adjoint system, bilinear inner form, eigenvectors, center manifold reduction, and normal form coefficients used in the main text for the analysis of properties of Hopf bifurcation at the threshold value of time delay $\omega_1 = \omega'_{11}$.

Assume $\tilde{p}_1 = S - S^*, \tilde{p}_2 = E - E^*, \tilde{p}_3 = I_1 - I_1^*, \tilde{p}_4 = I_2 - I_2^*, \tilde{p}_5 = H - H^*, \tilde{p}_6 = T - T^*, \tilde{p}_7 = R - R^*$ and $\omega_1 = \zeta + \omega'_{11}$, where $\zeta \in \mathbb{R}$. Further, normalize the time delay ω_1 by the scaling of time t as $t \to t/\omega_1$. Thus, system (2.1) attains the functional differential form as follows:

$$
\dot{\tilde{p}}(t) = F(\zeta, \tilde{p}_t) + L_\zeta(\tilde{p}_t), \tag{7.26}
$$

with $F : \mathbb{R} \times C \to \mathbb{R}^7$ and $L_\zeta : C \to \mathbb{R}^7$ are expressed as

$$
F(\zeta, \varphi) = \begin{pmatrix} 0 \\ -\alpha e^{-\mu\omega'_{11}}\varphi_1(-1)(\varphi_3(-1) + \varphi_4(-1)) \\ \alpha e^{-\mu\omega'_{11}}\varphi_1(-1)(\varphi_3(-1) + \varphi_4(-1)) \\ 0 \\ 0 \\ 0 \\ 0 \end{pmatrix},
$$

and

$$
L_\zeta\varphi = (\zeta + \omega'_{11})\left(\Delta_{1\max}\varphi(0) + \Delta_{2\max}\varphi\left(-\frac{\omega'_{22}}{\omega'_{11}}\right) + \Delta_{3\max}\varphi(-1)\right),
$$

with

$$\Delta_{1\max}=\begin{pmatrix} P_{11} & 0 & P_{13} & P_{14} & 0 & 0 & 0\\ P_{21} & P_{22} & P_{23} & P_{24} & 0 & 0 & 0\\ 0 & 0 & P_{33} & 0 & 0 & 0 & P_{37}\\ 0 & 0 & P_{43} & P_{44} & 0 & 0 & 0\\ 0 & 0 & 0 & P_{54} & P_{55} & 0 & 0\\ 0 & 0 & P_{63} & P_{64} & 0 & P_{66} & 0\\ 0 & 0 & 0 & 0 & P_{75} & P_{76} & P_{77} \end{pmatrix}, \quad \Delta_{2\max}=\begin{pmatrix} 0 & 0 & 0 & 0 & 0 & 0 & 0\\ 0 & 0 & 0 & 0 & 0 & 0 & 0\\ 0 & 0 & 0 & 0 & 0 & 0 & 0\\ 0 & 0 & 0 & 0 & 0 & 0 & R_{47}\\ 0 & 0 & 0 & 0 & 0 & 0 & 0\\ 0 & 0 & 0 & 0 & 0 & 0 & 0\\ 0 & 0 & 0 & 0 & 0 & 0 & R_{77} \end{pmatrix},$$

$$\Delta_{3\max}=\begin{pmatrix} 0 & 0 & 0 & 0 & 0 & 0 & 0\\ Q_{21} & 0 & Q_{23} & Q_{24} & 0 & 0 & 0\\ Q_{31} & 0 & Q_{33} & Q_{34} & 0 & 0 & 0\\ 0 & 0 & 0 & 0 & 0 & 0 & 0\\ 0 & 0 & 0 & 0 & 0 & 0 & 0\\ 0 & 0 & 0 & 0 & 0 & 0 & 0\\ 0 & 0 & 0 & 0 & 0 & 0 & 0 \end{pmatrix}.$$

By the Riesz representation theorem [37], there exists a function $\vartheta(\theta,\zeta)$, whose components are of bounded variation for $\theta\in[-1,0]$ such that

$$L_\zeta\varphi=\int_{-1}^{0} d\vartheta(\theta,\zeta)\varphi(\theta).$$

We can choose

$$\vartheta(\theta,\zeta)=\begin{cases} (\omega_{11}'+\zeta)(\Delta_{1\max}+\Delta_{2\max}+\Delta_{3\max}), & \theta=0,\\ (\omega_{11}'+\zeta)(\Delta_{2\max}+\Delta_{3\max}), & \theta\in\left[-\frac{\omega_{22}'}{\omega_{11}'},0\right),\\ (\omega_{11}'+\zeta)(\Delta_{3\max}), & \theta\in\left(-1,-\frac{\omega_{22}'}{\omega_{11}'}\right),\\ 0, & \theta=-1, \end{cases}$$

with $\delta(\theta)=\begin{cases} 0, & \theta\neq 0,\\ 1, & \theta=1. \end{cases}$

For $\varphi\in C([-1,0],\mathbb{R}^7)$, define

$$R(\zeta)\varphi=\begin{cases} 0, & -1\le\theta<0,\\ F(\zeta,\theta), & \theta=0, \end{cases}$$

and

$$A(\zeta)\varphi=\begin{cases} \frac{d\varphi(\theta)}{d\theta}, & -1\le\theta<0,\\ \int_{-1}^{0} d\vartheta(\theta,\zeta)\varphi(\theta), & \theta=0. \end{cases}$$

Thus, system (7.26) can be rewritten in the following equivalent form:

$$\dot{\tilde{p}}(t)=R(\zeta)\tilde{p}(t)+A(\zeta)\tilde{p}(t). \tag{7.27}$$

For $\kappa\in C'([0,1],(\mathbb{R}^7)^*)$ and $\varphi\in C([-1,0],\mathbb{R}^7)$, the bilinear inner form is defined as

$$\langle\kappa(s),\varphi(s)\rangle=\bar{\kappa}(0)\varphi(0)-\int_{\theta=-1}^{0}\int_{\nu=0}^{\theta}\bar{\kappa}(\nu-\theta)d\vartheta(\theta)\varphi(\nu)d\nu, \tag{7.28}$$

where $\vartheta(\theta)=\vartheta(\theta,0)$. For $\kappa\in C'([0,1],(\mathbb{R}^7)^*)$, the adjoint operator of $A(0)$ is expressed as

$$A^*(\kappa)=\begin{cases} -\frac{d\kappa(s)}{ds}, & 0<s\le 1,\\ \int_{-1}^{0} d\vartheta^T(s,0)\kappa(-s), & s=0. \end{cases}$$

From previous section, it can be observed that $\pm i\omega'_{11}p'$ are the eigenvalues of $A(0)$, so $\pm i\omega'_{11}p'$ are also the eigenvalues of $A^*(0)$. Let $p(\theta) = (1, p_2, p_3, p_4, p_5, p_6, p_7)^T e^{i\omega'_{11}p'\theta}$ and $p^*(s) = D(1, p_2^*, p_3^*, p_4^*, p_5^*, p_6^*, p_7^*)^T e^{i\omega'_{11}p's}$ be the eigenvectors of $A(0)$ and $A^*(0)$ corresponding to the eigenvalues $+i\omega'_{11}p'$ and $-i\omega'_{11}p'$, respectively. Hence, we obtain

$$
\begin{aligned}
p_2 =& \frac{-(P_{21} + Q_{21}e^{-ip'\omega_{11}}) - (P_{23} + Q_{23}e^{-ip'\omega_{11}})p_3 - (P_{24} + Q_{24}e^{-ip'\omega_{11}})p_4}{(P_{22} - ip')},\\
p_3 =& \frac{-P_{14}p_4 - (P_{11} - ip')}{P_{13}}, \quad p_4 = \frac{-Q_{31}e^{-ip'\omega_{11}} - (P_{33} + Q_{33}e^{-ip'\omega_{11}} - ip')p_3 - P_{37}p_7}{Q_{34}e^{-ip'\omega_{11}}},\\
p_5 =& \frac{-P_{54}p_4}{(P_{55} - ip')}, \; p_6 = \frac{-P_{63}p_3 - P_{64}p_4}{(P_{66} - ip')}, \quad p_7 = \frac{-P_{43}p_3 - (P_{44} - ip')p_4}{R_{47}e^{-ip'\omega'_{22}}},\\
p_2^* =& \frac{-(P_{11} + ip') - Q_{31}e^{ip'\omega_{11}}p_3^*}{P_{21} + Q_{21}e^{ip'\omega_{11}}}, \quad p_3^* = \frac{-P_{13} - (P_{23} + Q_{23}e^{ip'\omega_{11}})p_2^* - P_{43}p_4^* - P_{63}p_6^*}{(P_{33} + Q_{33}e^{ip'\omega'_{11}} + ip')},\\
p_4^* =& \frac{-P_{14} - (Q_{34}e^{ip'\omega'_{11}})p_3^* - (P_{24} + Q_{24}e^{ip'\omega'_{11}})p_2^* - P_{54}p_5^* - P_{64}p_6^*}{P_{44} + ip'},\\
p_5^* =& \frac{-P_{75}p_7^*}{(P_{55} + ip')}, \; p_6^* = \frac{-P_{76}p_7^*}{(P_{66} + ip')}, \quad p_7^* = \frac{-R_{47}e^{ip'\omega'_{22}}p_4^* - P_{37}p_3^*}{P_{77} + R_{47}e^{ip'\omega'_{22}} + ip'}.
\end{aligned}
$$

To prove $\langle p^*, \bar{p}\rangle = 0$ and $\langle p^*, p\rangle = 1$, we first require to calculate the value of $\bar{D}$. Considering Eq. (7.28), we choose

$$
\begin{aligned}
\bar{D} =& [1 + \sum_{i=2}^{7} p_i\bar{p}_i^* + \omega'_{11}e^{-i\omega'_{11}p'}((Q_{21}\bar{p}_2^* + Q_{31}\bar{p}_3^*) + p_3(Q_{23}\bar{p}_2^* + Q_{33}\bar{p}_3^*)\\
&+ p_4(Q_{24}\bar{p}_2^* + Q_{34}\bar{p}_3^*)) + \omega'_{22}e^{-i\omega'_{22}p'}p_7(R_{47}\bar{p}_4^* + R_{77}\bar{p}_7^*)]^{-1}.
\end{aligned}
$$

Here, we use the similar notations as in Hassard et al. [36] and calculate the coordinates to describe the center manifold C_0 at $\zeta = 0$. Let $\tilde{p}_t$ be the solution of Eq. (7.26), when $\zeta = 0$. Define

$$
z(t) = \langle p^*, \tilde{p}_t\rangle, \quad W(t,\theta) = \tilde{p}_t(\theta) - 2Re\left\{z(t)p(\theta)\right\}. \tag{7.29}
$$

On the center manifold C_0, we have

$$
W(t,\theta) = W(z(t), \bar{z}(t), \theta),
$$

where

$$
\begin{aligned}
W(z(t), \bar{z}(t), \theta) =& W(z, \bar{z}),\\
=& W_{20}(\theta)\frac{z^2}{2} + W_{11}(\theta)z\bar{z} + W_{02}(\theta)\frac{\bar{z}^2}{2} + W_{30}(\theta)\frac{z^3}{2} + \dots,
\end{aligned}
$$

and z and $\bar{z}$ are local coordinates for center manifold C_0 in the direction of p^* and $\bar{p}^*$. Note that W is also real if $\tilde{p}_t$ is real, we consider only real solutions. For solutions $\tilde{p}_t \in C_0$ of Eq. (7.26), since $\zeta = 0$,

$$
\begin{aligned}
\dot{z}(t) =& i\omega'_{11}p'z + \bar{p}^*(0)F(0, W(z,\bar{z},\theta)) + 2Re\left\{z(t)p(\theta)\right\},\\
=& i\omega'_{11}p'z + g(z,\bar{z}),
\end{aligned}
$$

where

$$
g(z,\bar{z}) = g_{20}\frac{z^2}{2} + g_{11}z\bar{z} + g_{02}\frac{\bar{z}^2}{2} + g_{21}\frac{z^2\bar{z}}{2} + \dots, \tag{7.30}
$$

then it follows from Eq. (7.26), that

$$\begin{aligned}\tilde{p}_t =& W(t,\theta) + 2Re\left\{z(t)p(\theta)\right\},\\ =& W_{20}(\theta)\frac{z^2}{2} + W_{11}(\theta)z\bar{z} + W_{02}(\theta)\frac{\bar{z}^2}{2} + (1,p_2,p_3,p_4,p_5,p_6,p_7)e^{i\omega'_{11}p'\theta}z\\ &+ (1,\bar{p}_2,\bar{p}_3,\bar{p}_4,\bar{p}_5,\bar{p}_6,\bar{p}_7)e^{-i\omega'_{11}p'\theta}\bar{z} + \dots.\end{aligned}$$

Hence, we have

$$\begin{aligned}g(z,\bar{z}) =& \bar{p}^*(0)F(0,\tilde{p}_t),\\ =& \bar{D}\omega'_{11}\Bigg[-\alpha e^{-\mu\omega'_{11}}p_2^*\Bigg(2(p_3+p_4)\frac{z^2}{2} + (p_3+p_4+\bar{p}_3+\bar{p}_4)z\bar{z} + 2(p_3+p_4)\frac{\bar{z}^2}{2}\\ &+\Big(W_{20}^{(1)}(-1)\bar{p}_3 + W_{20}^{(1)}(-1)\bar{p}_4 + W_{20}^{(3)}(-1) + W_{20}^{(4)}(-1) + 2W_{11}^{(3)}(-1)\\ &+2W_{11}^{(4)}(-1) + 2W_{11}^{(1)}(-1)p_3 + 2W_{11}^{(1)}(-1)p_4\Big)\frac{z^2\bar{z}}{2} + \dots\Bigg)\\ &+\alpha e^{-\mu\omega'_{11}}p_3^*\Bigg(2(p_3+p_4)\frac{z^2}{2} + (p_3+p_4+\bar{p}_3+\bar{p}_4)z\bar{z} + 2(p_3+p_4)\frac{\bar{z}^2}{2}\\ &+\Big(W_{20}^{(1)}(-1)\bar{p}_3 + W_{20}^{(1)}(-1)\bar{p}_4 + W_{20}^{(3)}(-1) + W_{20}^{(4)}(-1) + 2W_{11}^{(3)}(-1)\\ &+2W_{11}^{(4)}(-1) + 2W_{11}^{(1)}(-1)p_3 + 2W_{11}^{(1)}(-1)p_4\Big)\frac{z^2\bar{z}}{2} + \dots\Bigg)\Bigg].\end{aligned}$$

Comparing the coefficients with (7.30), we obtain

$$\begin{aligned}g_{20} =& \bar{D}\omega'_{11}\alpha e^{-\mu\omega'_{11}}2(p_3+p_4)(p_3^*-p_2^*),\\ g_{11} =& \bar{D}\omega'_{11}\alpha e^{-\mu\omega'_{11}}(p_3+p_4+\bar{p}_3+\bar{p}_4)(p_3^*-p_2^*),\\ g_{02} =& \bar{D}\omega'_{11}\alpha e^{-\mu\omega'_{11}}2(\bar{p}_3+\bar{p}_4)(p_3^*-p_2^*),\\ g_{21} =& \bar{D}\omega'_{11}\alpha e^{-\mu\omega'_{11}}\Big(W_{20}^{(1)}(-1)\bar{p}_3 + W_{20}^{(1)}(-1)\bar{p}_4 + W_{20}^{(3)}(-1) + W_{20}^{(4)}(-1) + 2W_{11}^{(3)}(-1)\\ &+2W_{11}^{(4)}(-1) + 2W_{11}^{(1)}(-1)p_3 + 2W_{11}^{(1)}(-1)p_4\Big)(p_3^*-p_2^*),\end{aligned}$$

with

$$\begin{aligned}W_{20}(\theta) =& \frac{ig_{20}p(0)}{\omega'_{11}p'}e^{i\omega'_{11}p'\theta} + \frac{i\bar{g}_{02}\bar{p}(0)}{3\omega'_{11}p'}e^{-i\omega'_{11}p'\theta} + E_1e^{2i\omega'_{11}p'\theta},\\ W_{11}(\theta) =& -\frac{ig_{11}p(0)}{\omega'_{11}p'}e^{i\omega'_{11}p'\theta} + \frac{i\bar{g}_{11}\bar{p}(0)}{\omega'_{11}p'}e^{-i\omega'_{11}p'\theta} + E_2.\end{aligned}$$

E_1 and E_2 can be determined by the following equations

$$E_1 = 2\begin{pmatrix} P_{11}^* & 0 & -P_{13} & -P_{14} & 0 & 0 & 0\\ P_{21}^* & P_{22}^* & P_{23}^* & P_{24}^* & 0 & 0 & 0\\ Q_{31}^* & 0 & P_{33}^* & Q_{34}^* & 0 & 0 & -P_{37}\\ 0 & 0 & -P_{43} & P_{44}^* & 0 & 0 & R_{47}^*\\ 0 & 0 & 0 & -P_{54} & P_{55}^* & 0 & 0\\ 0 & 0 & -P_{63} & -P_{64} & 0 & P_{66}^* & 0\\ 0 & 0 & 0 & 0 & -P_{75} & -P_{76} & P_{77}^* \end{pmatrix}^{-1} \times \begin{pmatrix} 0\\ E'_{11}\\ E'_{21}\\ 0\\ 0\\ 0\\ 0 \end{pmatrix},$$

$$E_2 = -\begin{pmatrix} P_{11} & 0 & P_{13} & P_{14} & 0 & 0 & 0 \\ P_{21}+Q_{21} & P_{22} & P_{23}+Q_{23} & P_{24}+Q_{24} & 0 & 0 & 0 \\ Q_{31} & 0 & P_{33}+Q_{33} & Q_{34} & 0 & 0 & P_{37} \\ 0 & 0 & P_{43} & P_{44} & 0 & 0 & R_{47} \\ 0 & 0 & 0 & P_{54} & P_{55} & 0 & 0 \\ 0 & 0 & P_{63} & P_{64} & 0 & P_{66} & 0 \\ 0 & 0 & 0 & 0 & P_{75} & P_{76} & P_{77}+R_{77} \end{pmatrix}^{-1} \times \begin{pmatrix} 0 \\ E'_{31} \\ E'_{41} \\ 0 \\ 0 \\ 0 \\ 0 \end{pmatrix},$$

where

$$\begin{aligned}
P^*_{11} =& 2ip' - P_{11},\ P^*_{22} = 2ip' - P_{22}, \\
P^*_{33} =& 2ip' - P_{33} - Q_{33}e^{-2i\omega'_{11}p'},\ P^*_{44} = 2ip' - P_{44}, \\
P^*_{55} =& 2ip' - P_{55},\ P^*_{66} = 2ip' - P_{66},\ P^*_{77} = 2ip' - P_{77} - R_{77}e^{-2i\omega'_{11}p'}, \\
P^*_{21} =& -P_{21} - Q_{21}e^{-2i\omega'_{11}p'},\ P^*_{23} = -P_{23} - Q_{23}e^{-2i\omega'_{11}p'}, \\
P^*_{24} =& -P_{24} - Q_{24}e^{-2i\omega'_{11}p'},\ Q^*_{31} = -Q_{31}e^{-2i\omega'_{11}p'}, \\
Q^*_{34} =& -Q_{34}e^{-2i\omega'_{11}p'},\ R^*_{47} = -R_{47}e^{-2i\omega'_{11}p'},\ E'_{11} = -(p_3+p_4)\alpha e^{-\mu\omega'_{11}}, \\
E'_{21} =& (p_3+p_4)\alpha e^{-\mu\omega'_{11}},\ E'_{31} = -(p_3+p_4+\bar{p}_3+\bar{p}_4)\alpha e^{-\mu\omega'_{11}}, \\
E'_{41} =& (p_3+p_4+\bar{p}_3+\bar{p}_4)\alpha e^{-\mu\omega'_{11}}.
\end{aligned}$$

Hence, we can determine the following values

$$\begin{aligned}
c_1(0) &= \frac{i}{2\omega'_{11}p'}\left(g_{20}g_{11} - 2|g_{11}|^2 - \frac{|g_{02}|^2}{3}\right) + \frac{g_{21}}{2}, \\
\mu_2 &= -\frac{Re\left\{c_1(0)\right\}}{Re\left\{\lambda'(\omega'_{11})\right\}}, \\
\beta_2 &= 2Re\left\{c_1(0)\right\}, \\
T_2 &= -\frac{Im\left\{c_1(0)\right\} + \mu_2 Im\left\{\lambda'(\omega'_{11})\right\}}{\omega'_{11}p'}.
\end{aligned}$$

Estimation of the length of time delays to sustain stability: Here, we present the detailed derivation of the linearized system, Laplace transform formulation, characteristic equation, and inequalities used to estimate the length of time delays to sustain stability by utilizing the Nyquist criterion [38].

Using the ensuing transformations $S = S^* + \tilde{p}_1, E = E^* + \tilde{p}_2, I_1 = I_1^* + \tilde{p}_3, I_2 = I_2^* + \tilde{p}_4, H = H^* + \tilde{p}_5, T = T^* + \tilde{p}_6, R = R^* + \tilde{p}_7$, we obtain the linearized system as follows:

$$\begin{aligned}
\frac{d\tilde{p}_1}{dt} =& a_{11}\tilde{p}_1 + a_{13}\tilde{p}_3, \\
\frac{d\tilde{p}_2}{dt} =& a_{21}\tilde{p}_1 + a_{22}\tilde{p}_2 + a_{23}\tilde{p}_3 + a_{24}\tilde{p}_4 + b_{21}\tilde{p}_1(t-\omega_1) + b_{23}\tilde{p}_3(t-\omega_1) + b_{24}\tilde{p}_4(t-\omega_1), \\
\frac{d\tilde{p}_3}{dt} =& a_{33}\tilde{p}_3 + a_{37}\tilde{p}_7 + b_{31}\tilde{p}_1(t-\omega_1) + b_{33}\tilde{p}_3(t-\omega_1) + b_{34}\tilde{p}_4(t-\omega_1), \\
\frac{d\tilde{p}_4}{dt} =& a_{43}\tilde{p}_3 + a_{44}\tilde{p}_4 + c_{47}\tilde{p}_7(t-\omega_2), \\
\frac{d\tilde{p}_5}{dt} =& a_{54}\tilde{p}_4 + a_{55}\tilde{p}_5, \\
\frac{d\tilde{p}_6}{dt} =& a_{63}\tilde{p}_3 + a_{64}\tilde{p}_4 + a_{66}\tilde{p}_6, \\
\frac{d\tilde{p}_7}{dt} =& a_{75}\tilde{p}_5 + a_{76}\tilde{p}_6 + a_{77}\tilde{p}_7 + c_{77}\tilde{p}_7(t-\omega_2),
\end{aligned} \tag{7.31}$$

where

$$
\begin{aligned}
a_{11} =& -(\mu+\alpha I_1^*),\ a_{13}=-\alpha S^*,\ a_{21}=\alpha(I_1^*+I_2^*),\ a_{22}=-\mu,\ a_{23}=a_{24}=\alpha S^*,\\
b_{21} =& \alpha(I_1^*+I_2^*)e^{-\mu\omega_1},\ b_{23}=b_{24}=-\alpha S^* e^{-\mu\omega_1},\ a_{33}=-(\tau_1+\gamma+\mu),\ a_{37}=\psi_1,\\
b_{31} =& -b_{21},\ b_{33}=b_{34}=-b_{23},\ a_{43}=\gamma,\ a_{44}=-(\tau_2+\xi+\mu+\delta),\ c_{47}=\psi_2 e^{-\mu\omega_2},\\
a_{54} =& \xi,\ a_{55}=-(\phi_H+\mu+\upsilon\delta),\ a_{63}=\tau_1,\ a_{64}=\tau_2,\ a_{66}=-(\phi_T+\mu),\\
a_{75} =& \phi_H,\ a_{76}=\phi_T,\ a_{77}=-(\mu+\psi_1),\ c_{77}=-c_{47}.
\end{aligned}
$$

We further obtain the following system by applying Laplace transform on system (7.31):

$$
\begin{aligned}
(s-a_{11})\overline{\tilde{p}_1}(s) =& \tilde{p}_1(0)+a_{13}\overline{\tilde{p}_3}(s),\\
(s-a_{22})\overline{\tilde{p}_2}(s) =& \tilde{p}_2(0)+a_{21}\overline{\tilde{p}_1}(s)+a_{23}\overline{\tilde{p}_3}(s)+a_{24}\overline{\tilde{p}_4}(s)+b_{21}e^{-s\omega_1}\overline{\tilde{p}_1}(s)\\
&+b_{21}e^{-s\omega_1}\bar{K}_1+b_{23}e^{-s\omega_1}\overline{\tilde{p}_3}(s)+b_{23}e^{-s\omega_1}\bar{K}_2+b_{24}e^{-s\omega_1}\overline{\tilde{p}_4}(s)\\
&+b_{24}e^{-s\omega_1}\bar{K}_3,\\
(s-a_{33}-b_{33}e^{-s\omega_1})\overline{\tilde{p}_3}(s) =& \tilde{p}_3(0)+a_{37}\overline{\tilde{p}_7}(s)+b_{31}e^{-s\omega_1}\overline{\tilde{p}_1}(s)+b_{31}e^{-s\omega_1}\bar{K}_1+b_{33}e^{-s\omega_1}\bar{K}_2\\
&+b_{34}e^{-s\omega_1}\overline{\tilde{p}_4}(s)+b_{34}e^{-s\omega_1}\bar{K}_3,\\
(s-a_{44})\overline{\tilde{p}_4}(s) =& \tilde{p}_4(0)+a_{43}\overline{\tilde{p}_3}(s)+c_{47}e^{-s\omega_2}\overline{\tilde{p}_7}(s)+c_{47}e^{-s\omega_2}\bar{K}_4,\\
(s-a_{55})\overline{\tilde{p}_5}(s) =& \tilde{p}_5(0)+a_{54}\overline{\tilde{p}_4}(s),\\
(s-a_{66})\overline{\tilde{p}_6}(s) =& \tilde{p}_6(0)+a_{63}\overline{\tilde{p}_3}(s)+a_{64}\overline{\tilde{p}_4}(s),\\
(s-a_{77}-c_{77}e^{-s\omega_2})\overline{\tilde{p}_7}(s) =& \tilde{p}_7(0)+a_{75}\overline{\tilde{p}_5}(s)+a_{76}\overline{\tilde{p}_6}(s)+c_{77}e^{-s\omega_2}\bar{K}_4.
\end{aligned}
\tag{7.32}
$$

where $\bar{K}_1=\int_{-\omega_1}^{0}e^{-s\omega_1}\tilde{p}_1(t)dt$, $\bar{K}_2=\int_{-\omega_1}^{0}e^{-s\omega_1}\tilde{p}_3(t)dt$, $\bar{K}_3=\int_{-\omega_1}^{0}e^{-s\omega_1}\tilde{p}_4(t)dt$, $\bar{K}_4=\int_{-\omega_2}^{0}e^{-s\omega_2}\tilde{p}_7(t)dt$, and $\overline{\tilde{p}_i}(s)$ are the Laplace transform of $\tilde{p}_i(t), i=1,2,3,4,5,6,7$ respectively. The characteristic equation of Eq. (7.32) is

$$
\begin{aligned}
\Xi(s) = u_0+u_1\lambda+&u_2\lambda^2+u_3\lambda^3+u_4\lambda^4+u_5\lambda^5+\lambda^6\\
&+(v_0+v_1\lambda+v_2\lambda^2+v_3\lambda^3+v_4\lambda^4+v_5\lambda^5)e^{-\lambda\omega_1}\\
&+(w_0+w_1\lambda+w_2\lambda^2+w_3\lambda^3+w_4\lambda^4+w_5\lambda^5)e^{-\lambda\omega_2}\\
&+(x_0+x_1\lambda+x_2\lambda^2+x_3\lambda^3+x_4\lambda^4)e^{-\lambda(\omega_1+\omega_2)},
\end{aligned}
\tag{7.33}
$$

where $u_i, v_i, w_i, i=0,1,2,3,4,5$, and $x_i, i=0,1,2,3,4$, are provided in the previous section. Local stability of D^* follows if

$$
Re(\Xi(i\eta_0))=0, \tag{7.34}
$$

$$
Im(\Xi(i\eta_0))>0, \tag{7.35}
$$

where η_0 is the smallest positive root of Eq. (7.34).

We further ponder the conditions: $\omega_1>0$ and ω_2 is in its stable interval, as of in case 8. Eqs. (7.34) and (7.35) gives

$$
c_6 = a_6\cos(p_5\omega_1)+b_6\sin(p_5\omega_1) \tag{7.36}
$$

$$
d_6 > b_6\cos(p_5\omega_1)-a_6\sin(p_5\omega_1), \tag{7.37}
$$

where a_6, b_6, c_6, and d_6 are given in the previous section. From (7.36), we have

$$
\begin{aligned}
u_4\eta_0^4 =& \cos(\eta_0\omega_1)(\eta_0^2v_2-\eta_0^4v_4-v_0)+\sin(\eta_0\omega_1)(\eta_0^3v_3-\eta_0^5v_5-\eta_0v_1)\\
&+\cos(\eta_0\omega_2)(\eta_0^2w_2-\eta_0^4w_4-w_0)+\sin(\eta_0\omega_2)(\eta_0^3w_3-\eta_0^5w_5-\eta_0w_1)\\
&+\cos(\eta_0\omega_1)\cos(\eta_0\omega_2)(\eta_0^2x_2-\eta_0^4x_4-x_0)+\sin(\eta_0\omega_1)\sin(\eta_0\omega_2)(\eta_0^4x_4-\eta_0^2x_2+x_0)\\
&+\sin(\eta_0\omega_1)\cos(\eta_0\omega_2)(\eta_0^3x_3-\eta_0x_1)+\sin(\eta_0\omega_2)\cos(\eta_0\omega_1)(\eta_0^3x_3-\eta_0x_1)+\eta_0^6+\eta_0^2u_2-u_0.
\end{aligned}
\tag{7.38}
$$

Maximize the right hand side of Eq. (7.38) subject to $|\sin(\eta_0\omega_1)| \leq 1, |\sin(\eta_0\omega_2)| \leq 1, |\cos(\eta_0\omega_1)| \leq 1, |\cos(\eta_0\omega_2)| \leq 1$, we obtain

$$\begin{aligned} u_4\eta_0^4 \leq & |\eta_0^2 v_2 - \eta_0^4 v_4 - v_0| + |\eta_0^3 v_3 - \eta_0^5 v_5 - \eta_0 v_1| + |\eta_0^2 w_2 - \eta_0^4 w_4 - w_0| \\ & + |\eta_0^3 w_3 - \eta_0^5 w_5 - \eta_0 w_1| + |\eta_0^2 x_2 - \eta_0^4 x_4 - x_0| + |\eta_0^4 x_4 - \eta_0^2 x_2 + x_0| \\ & + |\eta_0^3 x_3 - \eta_0 x_1| + |\eta_0^3 x_3 - \eta_0 x_1| + |\eta_0^6 + \eta_0^2 u_2 - u_0|. \end{aligned} \tag{7.39}$$

Let Eq. (7.39) has a positive root such that $\eta_0 \leq \eta^+$. Now, rearranging the inequality (7.37), we obtain

$$\begin{aligned} \eta_0^4 \leq & \frac{\sin(\eta_0\omega_1)(\eta_0^4 v_4 - \eta_0^2 v_2 + v_0)}{\eta_0 u_5} + \frac{\cos(\eta_0\omega_1)(\eta_0^5(-v_5) + \eta_0^3 v_3 - \eta_0 v_1)}{\eta_0 u_5} \\ & + \frac{\cos(\eta_0\omega_2)(\eta_0^3 w_3 - \eta_0^5 w_5 - \eta_0 w_1)}{\eta_0 u_5} + \frac{\sin(\eta_0\omega_2)(\eta_0^4 w_4 - \eta_0^2 w_2 + w_0) + \eta_0^3 u_3 - \eta_0 u_1}{\eta_0 u_5} \\ & + \frac{\sin(\eta_0\omega_1)\cos(\eta_0\omega_2)(\eta_0^4 x_4 - \eta_0^2 x_2 + x_0)}{\eta_0 u_5} + \frac{\sin(\eta_0\omega_2)\cos(\eta_0\omega_1)(\eta_0^4 x_4 - \eta_0^2 x_2 + x_0)}{\eta_0 u_5} \\ & + \frac{\cos(\eta_0\omega_1)\cos(\eta_0\omega_2)(\eta_0^3 x_3 - \eta_0 x_1)}{\eta_0 u_5} + \frac{\sin(\eta_0\omega_1)\sin(\eta_0\omega_2)(\eta_0 x_1 - \eta_0^3 x_3)}{\eta_0 u_5}. \end{aligned} \tag{7.40}$$

Substituting Eq. (7.38) in Eq. (7.40), assuming $|\sin(\eta_0\omega_2)| \leq 1, |\cos(\eta_0\omega_2)| \leq 1$, and rearranging, we obtain

$$2\sin^2\left(\frac{\eta_0\omega_1}{2}\right)\tilde{K}_{11}(\eta_0) + \sin(\eta_0\omega_1)\tilde{K}_{12}(\eta_0) \leq \tilde{K}_{13}(\eta_0), \tag{7.41}$$

where

$$\begin{aligned} \tilde{K}_{11}(\eta_0) = & \eta_0 u_5(\eta_0^4(-v_4) + \eta_0^2 v_2 - v_0) - |u_4(\eta_0^5(-v_5) + \eta_0^3 v_3 - \eta_0 v_1)| - |u_4(\eta_0 x_1 - \eta_0^3 x_3)| \\ & - |u_4(\eta_0^4 x_4 - \eta_0^2 x_2 + x_0)| - |\eta_0 u_5(\eta_0 x_1 - \eta_0^3 x_3)| - |\eta_0 u_5(\eta_0^4 x_4 - \eta_0^2 x_2 + x_0)|, \\ \tilde{K}_{12}(\eta_0) = & \eta_0(-u_5)(\eta_0^5 v_5 - \eta_0^3 v_3 + \eta_0 v_1) - |u_4(\eta_0^4 v_4 - \eta_0^2 v_2 + v_0)| - |u_4(\eta_0 x_1 - \eta_0^3 x_3)| \\ & - |u_4(\eta_0^4 x_4 - \eta_0^2 x_2 + x_0)| - |\eta_0 u_5(\eta_0 x_1 - \eta_0^3 x_3)| - |\eta_0 u_5(\eta_0^4 x_4 - \eta_0^2 x_2 + x_0)|, \\ \tilde{K}_{13}(\eta_0) = & |u_4(\eta_0^3 u_3 - \eta_0 u_1)| + |\eta_0 u_5(\eta_0^6 + \eta_0^2 u_2 - u_0)| + |\eta_0 u_5(\eta_0^4 w_4 - \eta_0^2 w_2 + w_0)| \\ & + |\eta_0 u_5(\eta_0^5 w_5 - \eta_0^3 w_3 + \eta_0 w_1)| + |u_4(\eta_0^4 w_4 - \eta_0^2 w_2 + w_0)| \\ & + |u_4(\eta_0^5 w_5 - \eta_0^3 w_3 + \eta_0 w_1)| - \eta_0 u_5(\eta_0^4(-v_4) + \eta_0^2 v_2 - v_0) \\ & + |u_4(\eta_0^5(-v_5) + \eta_0^3 v_3 - \eta_0 v_1)| + |u_4(\eta_0 x_1 - \eta_0^3 x_3)| + |u_4(\eta_0^4 x_4 - \eta_0^2 x_2 + x_0)| \\ & + |\eta_0 u_5(\eta_0 x_1 - \eta_0^3 x_3)| + |\eta_0 u_5(\eta_0^4 x_4 - \eta_0^2 x_2 + x_0)|. \end{aligned}$$

Now, from inequality (7.41), we have

$$\tilde{K}_{11}(\eta^+)\omega_1^2 + \tilde{K}_{12}(\eta^+)\omega_1 \leq \tilde{K}_{13}(\eta^+), \tag{7.42}$$

where $\tilde{K}_{11}(\eta^+) = \frac{\eta^{+2}}{2}\left|\tilde{K}_{11}(\eta_0)\right|_{\eta_0=\eta^+}$, $\tilde{K}_{12}(\eta^+) = \eta^+\left|\tilde{K}_{12}(\eta_0)\right|_{\eta_0=\eta^+}$, $\tilde{K}_{13}(\eta^+) = \left(\tilde{K}_{13}(\eta_0)\right)_{\eta_0=\eta^+}$. Hence, if

$$\omega_1^+ = \frac{1}{2\tilde{K}_{11}(\eta^+)}\left(-\tilde{K}_{12}(\eta^+) + \sqrt{\tilde{K}_{12}^2(\eta^+) + 4\tilde{K}_{11}(\eta^+)\tilde{K}_{13}(\eta^+)}\right) \tag{7.43}$$

then the stability is preserved for $0 \leq \omega_1 < \omega_1^+$.

A similar procedure yields the length of time delay ω_2 where the stability is sustained, considering ω_1 in its stable interval.

Appendix C

Table 3: Effect of varying the relapse rate (ψ_1) on cumulative NiV incidence over 2001-2030.

% change	ψ_1	Cumulative cases	Cases averted	Reduction (%)
-30	1.378	306.76	49.10	13.80
-20	1.574	322.30	33.56	9.43
-10	1.770	338.61	17.26	4.85
Base value	1.968	355.87	0.00	0.00
+10	2.165	373.85	-17.98	-5.05
+20	2.362	392.63	-36.76	-10.33
+30	2.558	412.13	-56.26	-15.81

Table 4: Effect of varying the effective incubation delay (ω_1) on cumulative NiV over 2001-2030.

% change	ω_1	Cumulative cases	Cases averted	Reduction (%)
-30	2.012	273.00	82.86	23.29
-20	2.299	298.39	57.48	16.15
-10	2.587	325.84	30.03	8.44
Base value	2.874	355.87	0.00	0.00
+10	3.161	381.85	-25.98	-7.30
+20	3.449	404.18	-48.32	-13.58
+30	3.736	428.52	-72.65	-20.41

Table 5: Effect of varying the time delay in developing encephalitis after recovery (ω_2) on cumulative NiV over 2001-2030.

% change	ω_2	Cumulative cases	Cases averted	Reduction (%)
-30	3.786	345.15	10.71	3.01
-20	4.326	348.76	7.11	2.00
-10	4.867	352.26	3.61	1.01
Base value	5.408	355.87	0.00	0.00
+10	5.949	360.29	-4.42	-1.24
+20	6.490	366.39	-10.52	-2.96
+30	7.030	374.46	-18.60	-5.23

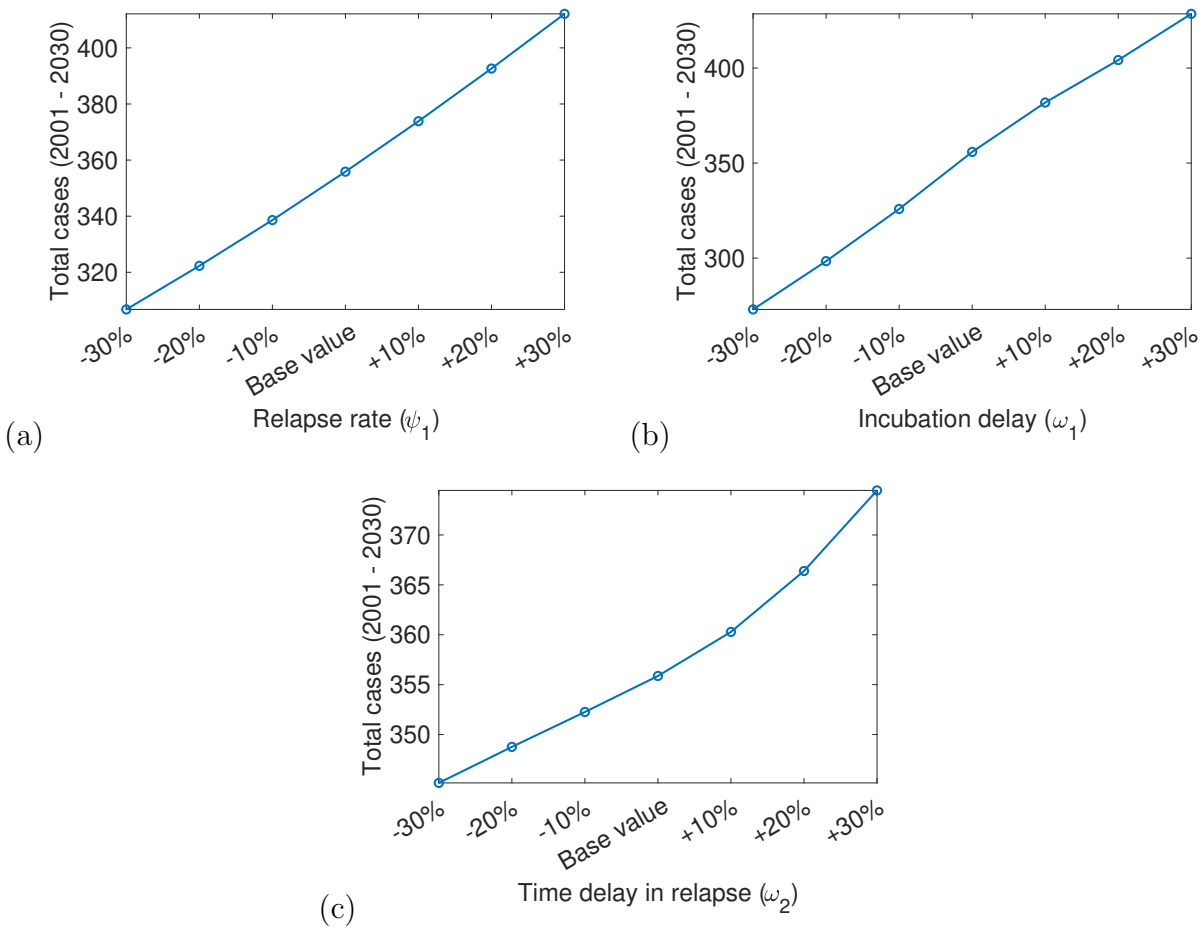

Figure 10: Total cumulative NiV cases over 2001 - 2030 under parameter perturbations. Panels show the cumulative number of cases generated by the model for varying values of (a) relapse rate (ψ_1), (b) incubation delay (ω_1), and (c) time delay in encephalitis development (ω_2), with all other parameters fixed at baseline values.

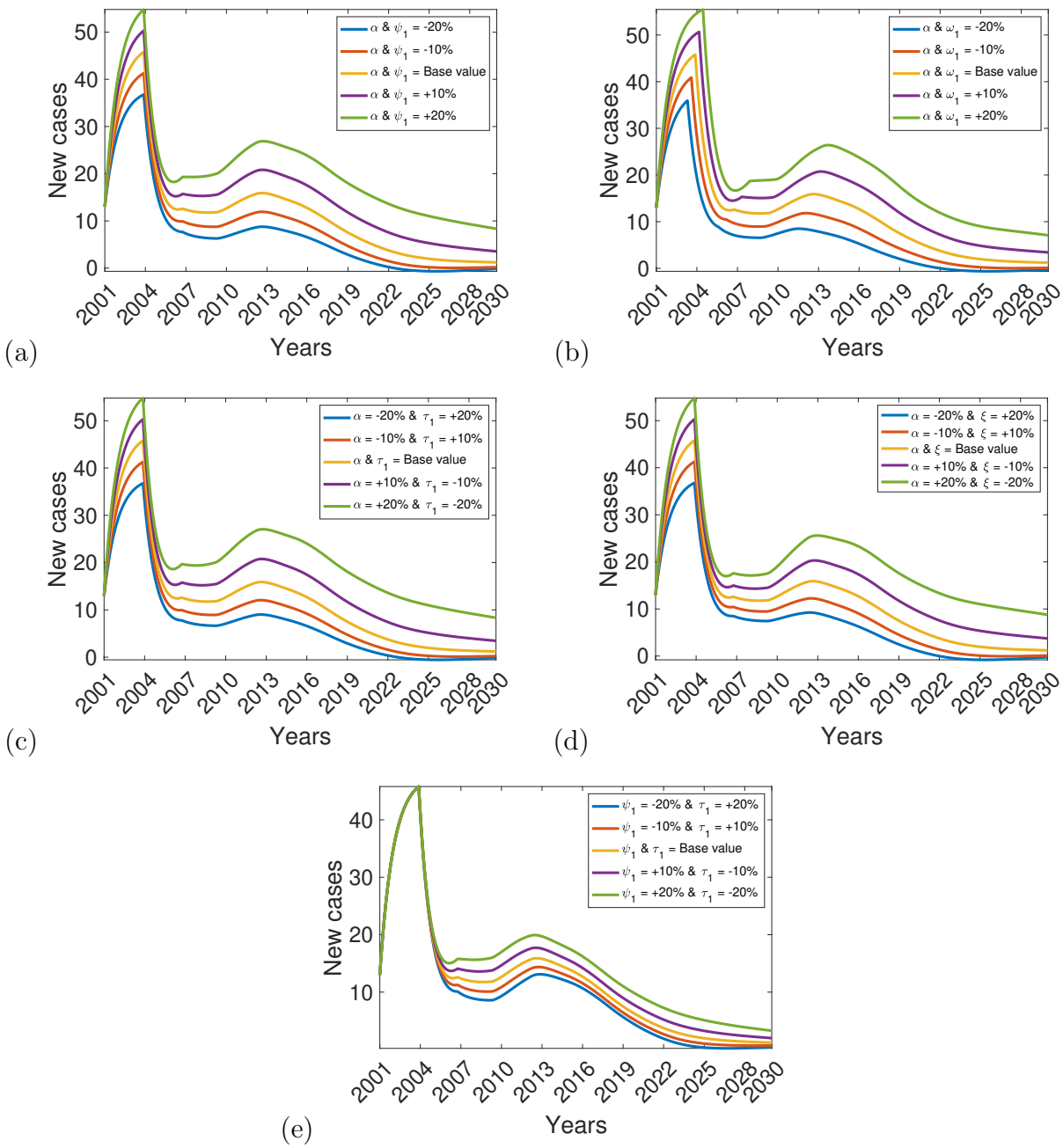

Figure 11: Time-series trajectories corresponding to the joint parameter perturbations underlying the sensitivity envelopes shown in Figure 6. Each panel displays model trajectories obtained by simultaneously varying two parameters within $\pm 20\%$ of their baseline values, while all other parameters are held fixed. Panels correspond to the following joint parameter combinations: (a) transmission rate (α) and relapse rate (ψ_1), (b) transmission rate (α) and incubation delay (ω_1), (c) transmission rate (α) and treatment rate of early-stage infectious individuals (τ_1), (d) transmission rate (α) and hospitalization rate of later-stage infectious individuals (ξ), and (e) relapse rate (ψ_1) and treatment rate of early-stage infectious individuals (τ_1). Individual trajectories differ in magnitude and timing, with the largest separation occurring during the later phase of the outbreak. Together, these trajectories illustrate the range of epidemic outcomes that define the envelope bounds presented in the main text.